Lawrence Berkeley National Laboratory
Recent Work

Title

A NUMERICAL and ANALYTICAL STUDY OF ANOMALOUS PROPAGATION OF ELECTRICAL IMPULSES IN DAMAGED HEART FIBERS

Permalink

https://escholarship.org/uc/item/3b21041p

Author

Miller, Robert

Publication Date

1976

LBL-4657
C.1

A NUMERICAL AND ANALYTICAL STUDY OF ANOMALOUS PROPAGATION OF ELECTRICAL IMPULSES IN DAMAGED HEART FIBERS

Robert Miller
(Ph. D. thesis)

January 1976

LBL-4657
C.1

DISCLAIMER

A NUMERICAL AND ANALYTICAL STUDY OF ANOMALOUS PROPAGATION

OF ELECTRICAL IMPULSES IN DAMAGED HEART FIBERS

Contents

LBL-4657

A NUMERICAL AND ANALYTICAL STUDY OF ANOMALOUS PROPAGATION

OF ELECTRICAL IMPULSES IN DAMAGED HEART FIBERS

Robert Miller
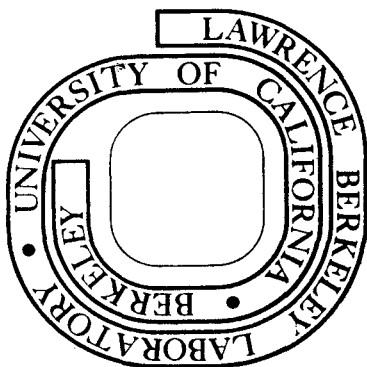
Lawrence Berkeley Laboratory
University of California
Berkeley, California 94720

Ph.D. Thesis

January 1976

ABSTRACT

The Purkinje fibers, which form the specialized electrical conduction
system of the heart, pose a challenge to the mathematical modeler. Their
electrical behavior resembles that of nervous tissue in several respects.
Small electrical stimuli elicit a response that is only detectable
locally, while injected currents whose magnitude exceeds a certain
threshold will produce a pulse that propagates the length of the fiber,
and whose shape is essentially independent of the applied stimulus. As
in the case of nerve fibers, the front of this pulse is very sharp,
characterized by rise times of the order of hundreds of microseconds,
and amplitudes of the order of 100 millivolts. The nerve pulse, however,
ends in a few milliseconds, while the Purkinje fiber membrane potential
remains nearly constant at a potential very far above the equilibrium
value for hundreds of milliseconds. This long excited state is called
the plateau. The long duration of the plateau compared to the times that

characterize the upstroke makes numerical simulations difficult, especially in the case of the partial differential equations that must be used to describe impulse propagation in spatially inhomogeneous fibers.

In this paper we investigate two sets of electrophysiological experiments on Purkinje fibers with the purpose of constructing a mathematical framework in which hypotheses about these experiments may be tested. Ultimately we hope to gain new insight into the working of the system that will aid in the design of new experiments.

First, we examine the experiments of Noble and Tsien (J. Physiol. 200 (1969) pp. 205-231) on the details of the current-voltage relations for the plateau of the action potential of the space-clamped Purkinje fiber. Their experimental data is used to construct a quantitative model of the electrical behavior of the membrane. We use this quantitative model to simulate the time course of the plateau, the abolition of the plateau (i.e., premature restoration of the equilibrium potential) by a hyperpolarizing shock, and the self-excited oscillations of the membrane potential at potentials in the plateau range which are observed in fibers that do not recover completely from the trauma of dissection.

Second, we examine the experimental results of Hoffman and Cranefield (Circ. Res. 28 (1971) pp. 199-219) on anomalous propagation effects in Purkinje fibers in which a portion of the length of the fiber is rendered inexcitable by encasing it in an agar block whose ionic composition differs greatly from that of the normal extracellular fluid. Observed in these experiments were long delays of conduction, one-way conduction, and the conduction of one impulse across the block for each group of two (or sometimes more, in some preparations) incident impulses. Adaptation of

0 0 0 4 5 0 0 4 3 0

-vii-

our quantitative ordinary differential equation model to a partial differ-
ential equation model to simulate these effects is conceptually complicated
and would be computationally expensive; hence, a simpler qualitative model
is derived. This model involves the injection of a current by a nonlinear
membrane element when the potential reaches a given threshold. This model
is then used to investigate the hypothesis that one-dimensional cable
theory and a plausible assumption about an asymmetry in the experimental
preparation are sufficient to explain the phenomena of delay and one-way
conduction. Specialized numerical techniques are derived to solve the
partial differential equations for the numerical experiments, and the
hypothesis of a one-dimensional cable is shown to be sufficient to predict
delay and one-way block. More powerful numerical techniques will be needed
to simulate one-for-n block with this model. The author and his coworkers
are currently developing such techniques.

A NUMERICAL AND ANALYTICAL STUDY OF ANOMALOUS PROPAGATION
OF ELECTRICAL IMPULSES IN DAMAGED HEART FIBERS

I. INTRODUCTION AND BACKGROUND

1. General Introduction

   This work presents a mathematical framework in which two sets of

experimental data can be understood. Two models will be described:

the first model is a set of ordinary differential equations whose solu-

tions reproduce in detail the behavior of the plateau of the Purkinje

fiber action potential as observed by Hauswirth, Noble and Tsien (12),

(16), (17); the second is a system of nonlinear partial differential

equations which is designed to reproduce qualitatively some of the anoma-

lous impulse propagation effects observed by Cranefield, Hoffman and

their co-workers in canine Purkinje fibers whose excitability had been

chemically depressed within small portions of their lengths.

   The parameters of the first model are derived by fitting polynomial

and piecewise linear functions to the measured relations of membrane

current to membrane potential and time found in (16) and (17). This

model will be seen to reproduce the self-excited oscillations observed in

fibers that do not recover from the dissection process as reported in (12).

The behavior of the second model in the case of spatial homogeneity will

be shown to be similar to that of the first model for the plateau of the

action potential for a healthy fiber, but it will not reproduce these

oscillations.

   We shall also examine in detail the numerical techniques for finding

approximate solutions to the ordinary and partial differential equations

from the models presented.

Let us begin with a brief review of the experimentally observed electrical characteristics of the Purkinje fibers. We adopt the following sign convention for the membrane potential and currents: the membrane potential will be said to increase as the interior becomes increasingly positive with respect to the exterior; the flow of positive charges inward is then regarded as a depolarizing current, and the flow of positive charges outward is a hyperpolarizing current.

2. Salient Features of the Electrical Behavior of Purkinje Fibers

The Purkinje fibers form the specialized conduction system of the heart. They are similar, but not identical to nerve fibers. Like nerve, and like most other heart or muscle tissue, they exhibit all or none response to electrical stimuli. The upstroke of the action potential (i.e. phase 1 of figure 13) has been shown to be mediated by sodium, with peak amplitude, conductance at peak amplitude, reversal potential and response to drugs similar to those of nerve cells (6). Like ventricular muscle and unlike nerve, Purkinje fibers exhibit a long plateau, often lasting hundreds of milliseconds after the initial rise. The plateau is stable with respect to small perturbations in potential, but may be abolished by strong hyperpolarizing currents.

The plateau has been studied experimentally by Noble and Tsien using voltage clamp techniques in which the membrane potential is held approximately constant in space and controlled in time, and the resulting currents measured (16), (17). These clamp techniques work well in the plateau region where the potential changes relatively slowly, but voltage

control is unreliable during the upstroke, and therefore the current vol-

tage relations are better understood for the plateau (6). The sequence

of events Noble and Tsien observe in (16) and (17) is as follows: after

the initial inward sodium current is inactivated, a depolarizing current

is activated that is responsible for the maintenance of the plateau itself.

A slowly activated outward current counteracts this current, and eventually

abolishes the plateau, restoring the potential of the interior of the cell

to its resting value approximately 100 millivolts below the exterior.

The experimental data from (16) were used to estimate the parameters

for the ODE's comprising the model presented in the next section.

$x_\infty(V)$ is the value that x approaches as t goes to ∞ if V is held constant; this function is derived from the experimental data in (16).

τ is the time constant in milliseconds associated with x. It is also estimated from experimental data.

$I(V)$ is the peak membrane current for a given value of V; this is the cubic polynomial referred to above; it has the dimensions of microamps/cm^2.

W is the total restoring current in microamps/cm^2.

W_0 is the fully activated value of the restoring current, measured in microamps/cm^2.

The experimental basis of this model of the plateau is described in (16). In (17), a model is presented, along with a numerical method for reconstructing the time course of the plateau from the voltage clamp data in (16). The numerical method is a graphical version of the explicit Cauchy-Euler scheme. The resulting numerical reconstruction is successful as far as it goes, but Noble and Tsien do not attempt to construct a formal mathematical model based upon their experimental data relating the time course of the membrane current to the membrane potential which is under their control. Actually, the graphs they use to evaluate the ionic currents and their activation levels are drawn by eye through a series of points; it is these points, not the curves that came directly from their experiments. Perhaps the actual fitting of analytic forms to the points would present some difficulty if the curve did not resemble any familiar function; but a glance at figures 7, 8, 9 and 11 in (16) (see appendix A, figures A1, A2, A3 and A4) reveals that a cubic polynomial

ought to provide a good fit to figure A4, a piecewise linear function should approximate A2 well, and as long as application of the model is restricted to the plateau range above -50 millivolts or so, A1 and A3 can be fitted by constants. On the basis of figures A1 and A3 constants were assigned for τ and for W_O for potentials in the plateau range, a least-squares cubic polynomial was fitted to A4, and a piecewise linear form for the function x was estimated from figure A2. We have thus essentially constructed an analytical form of Noble and Tsien's graphical theory. Because of the compromises made, this model will only reproduce the dynamics accurately in or near the plateau range; but the least-squares cubic fits the instantaneous voltage-current relation so well that the predicted resting potential of -80.73 mV. and resting conductance of 2.00898×10^{-4} mho/cm^2 compare quite favorably with measured values of -94 mV.(3, page 44) and 5.155×10^{-4} mho/cm^2(3, page 198).

The actual numbers derived from Noble and Tsien's data that determine the explicit form of (2.1) are:

$$I(V) = (9.283 \times 10^{-5}V^2 + .578 \times 10^{-2}V + .0706)(V + 80.73) \qquad (2.2)$$

$$x_\infty(V) = .01695V + .949, V \geqslant -55\text{mV} \qquad (2.3)$$

$$= 0, V < -55$$

$$\tau = 550\text{msec}$$

$$W_O = 8\mu A/\text{cm}^2 .$$

C will be taken to be 2.4 μF/cm^2, following Fozzard (10).

The dynamics of the fast sodium current that is responsible for the upstroke of the action potential are not included in this model; it has been noted above that reliable voltage clamp data are not available for

for the upstroke. The voltage clamp techniques used are too slow to follow

the Na current, and thus the steady state Na current is implicitly included

in I(V). Therefore this model can not be expected to produce action poten-

tials with the proper upstroke velocities. That the model will not produce

proper action potentials can be easily seen by examining (2.1). At the

resting potential, W = 0, and

$$\frac{dV}{dt} = \frac{-1}{C} I(V)$$

Taking the maximum of the right hand side indicates that the largest values

of dV/dt to be expected are in the range of 1 millivolt per millisecond,

two orders of magnitude smaller than typical upstroke velocities, but

quite satisfactory for the velocity of repolarization (16).

Numerical integration of (2.1) yields, as expected, simulated plateaus

that possess all of the desired characteristics. Figure 1 shows the time

course of a simulated plateau, beginning with initial conditions V = -10

and W = 0; notice the similarity to the experimentally observed response,

figure A5, from (3), page 177. Figure 2 illustrates the phenomenon of all

or none repolarization in the response of the model to a series of hyper-

polarizing shocks of increasing intensity. Four graphs are plotted: the

normal time course shown in figure 1, and the time courses of three simu-

lations that were subjected to hyperpolarizing shocks of 5, 10 and 12.5

microamps/cm^2 from t = 5 to t = 15 ms. Here, as in the real system, a

hyperpolarizing stimulus of a given duration will not abolish the plateau

unless its strength exceeds a certain threshold.

The phase portrait of the system (2.1) for the case of zero total

current is given in figure 3, where the nullclines for V and W (i.e.

those curves on which $\frac{dV}{dt}$ and $\frac{dW}{dt}$ respectively equal zero; their intersections

SIMULATED PLATEAU

FIGURE 1

ALL OR NONE REPOLARIZATION FROM PLATEAU

FIGURE 2

PHASE PORTRAIT FOR SYSTEM

RESTORING CURRENT, MICROAMPS/(SQ.CM)

MEMBRANE POTENTIAL, MV.

DOTTED LINES ARE ISOCLINES
SOLID LINES ARE TRAJECTORIES
CAPACITANCE = 2.4

FIGURE 3
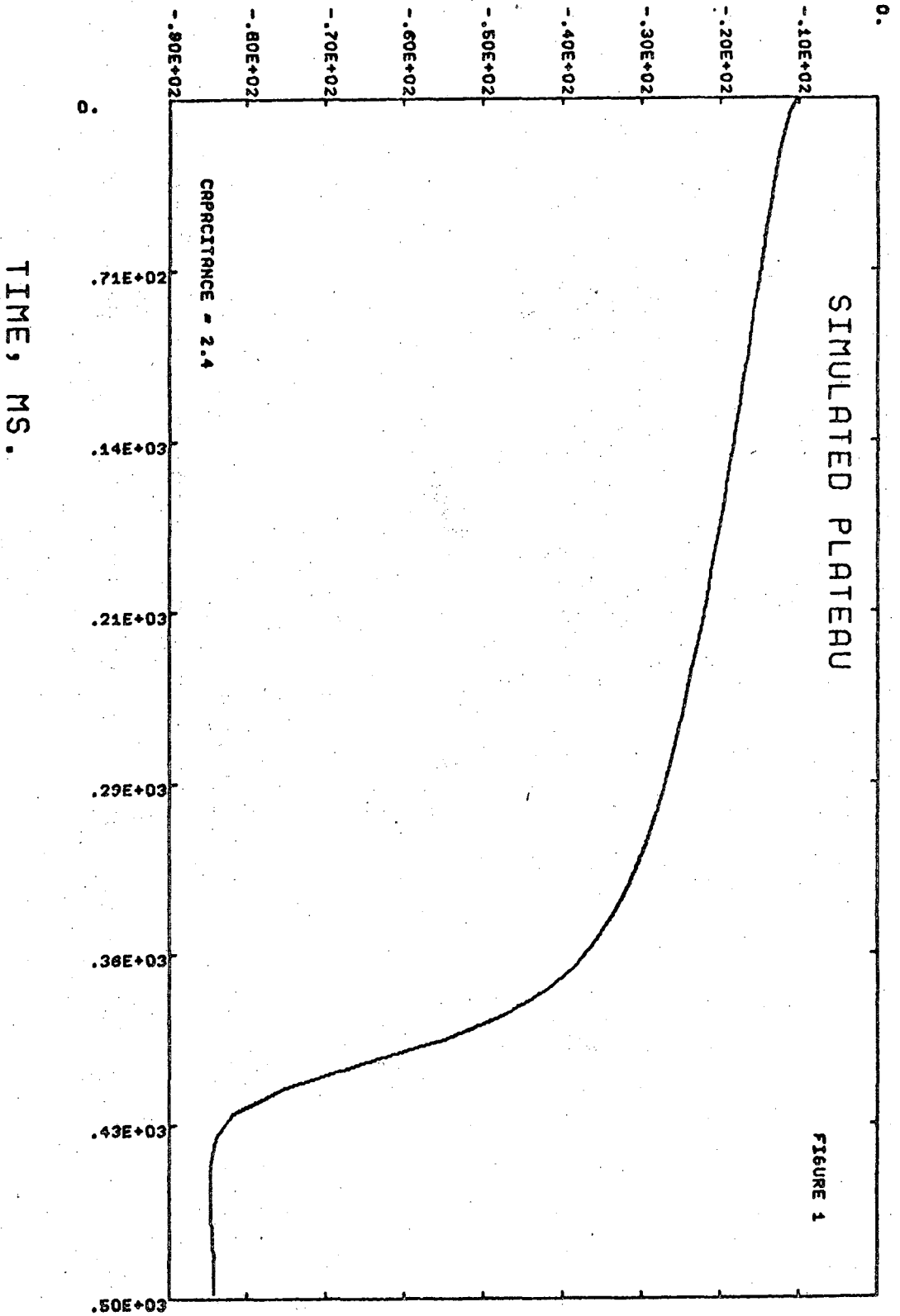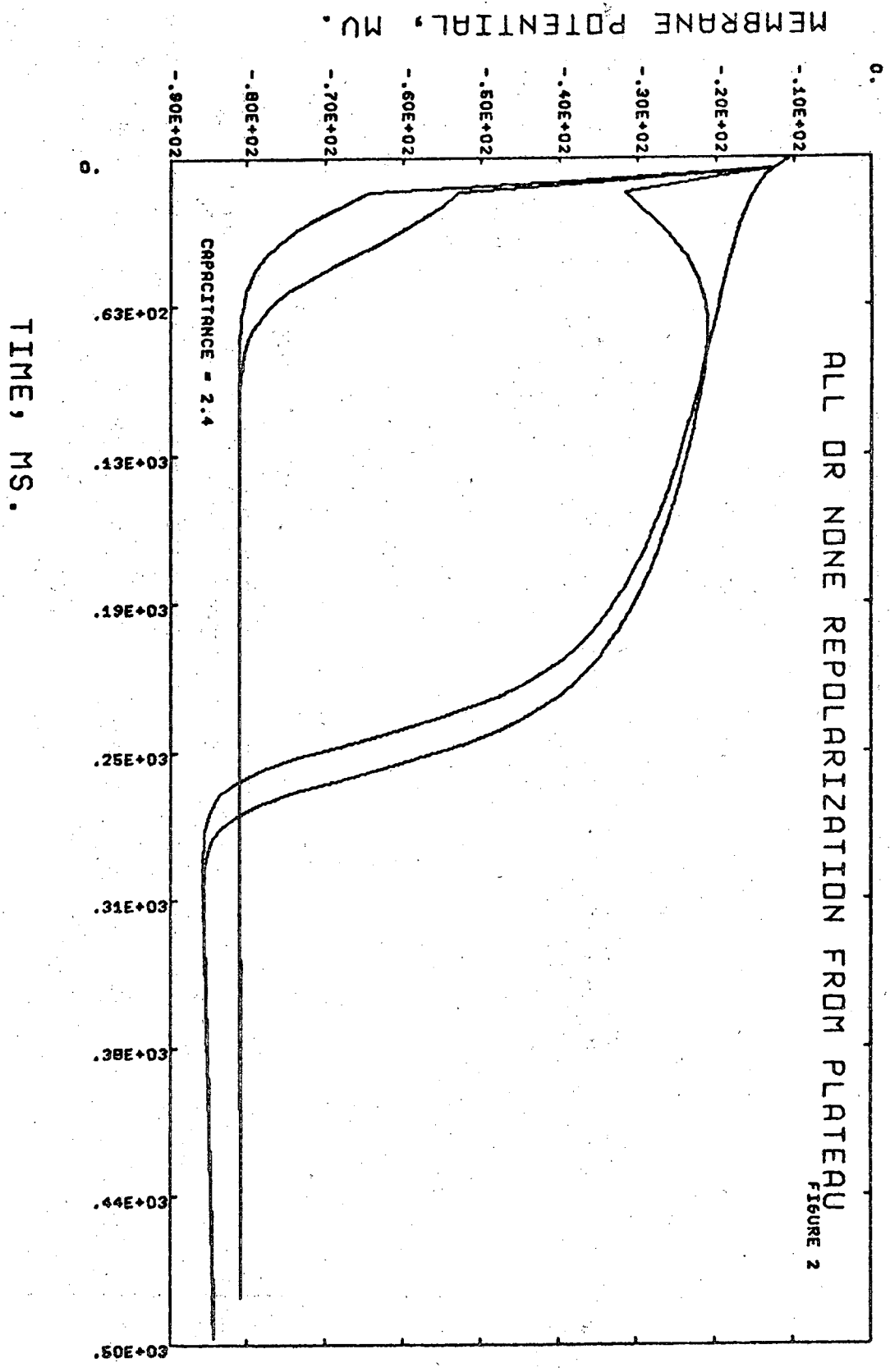
are the equilibrium points of the system.) are shown, along with several

representative trajectories. In terms of circuit theory, this model cor-

responds to a nonlinear conductor in parallel with a capacitor. The only
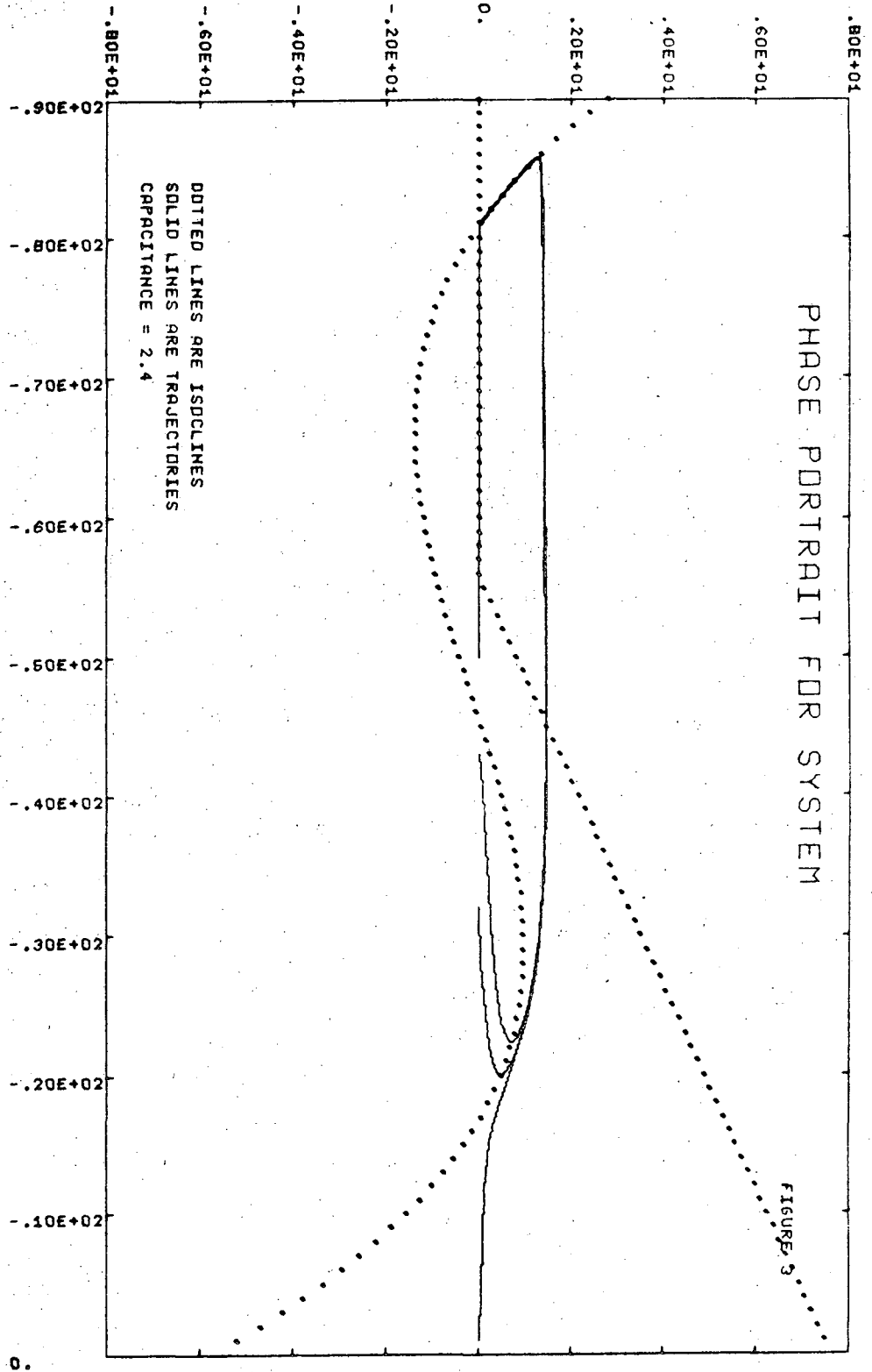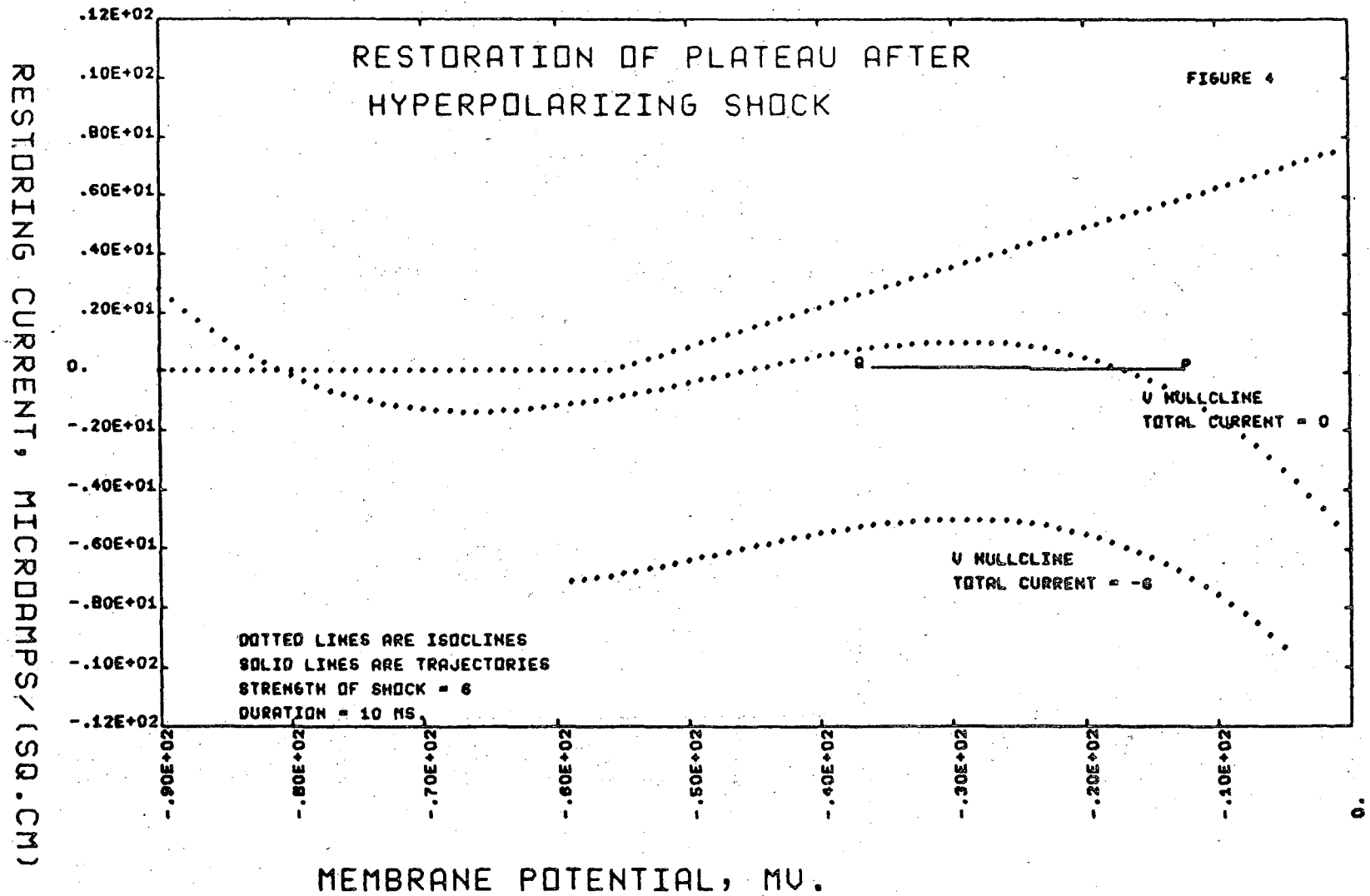
equilibrium point of this system is at $W = 0$, $V = -80.73$. This equilib-

rium point is a stable one, as expected.

All or nothing repolarization can be easily understood in terms of

the phase portrait. During the plateau, the potential is approximately

constant, so the portion of the trajectory in phase space corresponding

to the plateau occurs near the V nullcline. A hyperpolarizing current

applied to the system would be modeled by adding a negative term to i_{total}

in (2.1). The effect of this on the phase portrait would simply be the

translation of the V nullcline downwards with no change in its shape, as

shown in figure 4. Consider now the trajectories passing through the

point P in figure 4, in the two cases of zero total current and negative

(i.e. hyperpolarizing) current. The trajectory is steeper in the zero

current case, since in the negative current case P is further from the

V nullcline and therefore $\left| \dfrac{dV}{dt} \right|$ is larger while $\dfrac{dW}{dt}$ remains unchanged.

If the hyperpolarizing current is then turned off, the V nullcline returns

to its original position which may now be above the point Q. In the re-

gion below the V nullcline $\dfrac{dV}{dt}$ is positive; thus in this case a depolar-

izing current will flow and the plateau will be restored. If, on the

other hand, the hyperpolarizing current should be sustained long enough

for the situation illustrated in figure 5 to occur, then the trajectory

would reach the point R which lies in the region where $\dfrac{dV}{dt}$ is negative,

and the membrane would be repolarized to the resting potential. Therefore

a standard strength-duration curve could be plotted for all or nothing

RESTORATION OF PLATEAU AFTER HYPERPOLARIZING SHOCK

FIGURE 4

V NULLCLINE
TOTAL CURRENT = 0

V NULLCLINE
TOTAL CURRENT = -6

DOTTED LINES ARE ISOCLINES
SOLID LINES ARE TRAJECTORIES
STRENGTH OF SHOCK = 6
DURATION = 10 MS

RESTORING CURRENT, MICROAMPS/(SQ.CM)

MEMBRANE POTENTIAL, MV.

-12-

ABOLITION OF PLATEAU BY HYPERPOLARIZING SHOCK

FIGURE 6
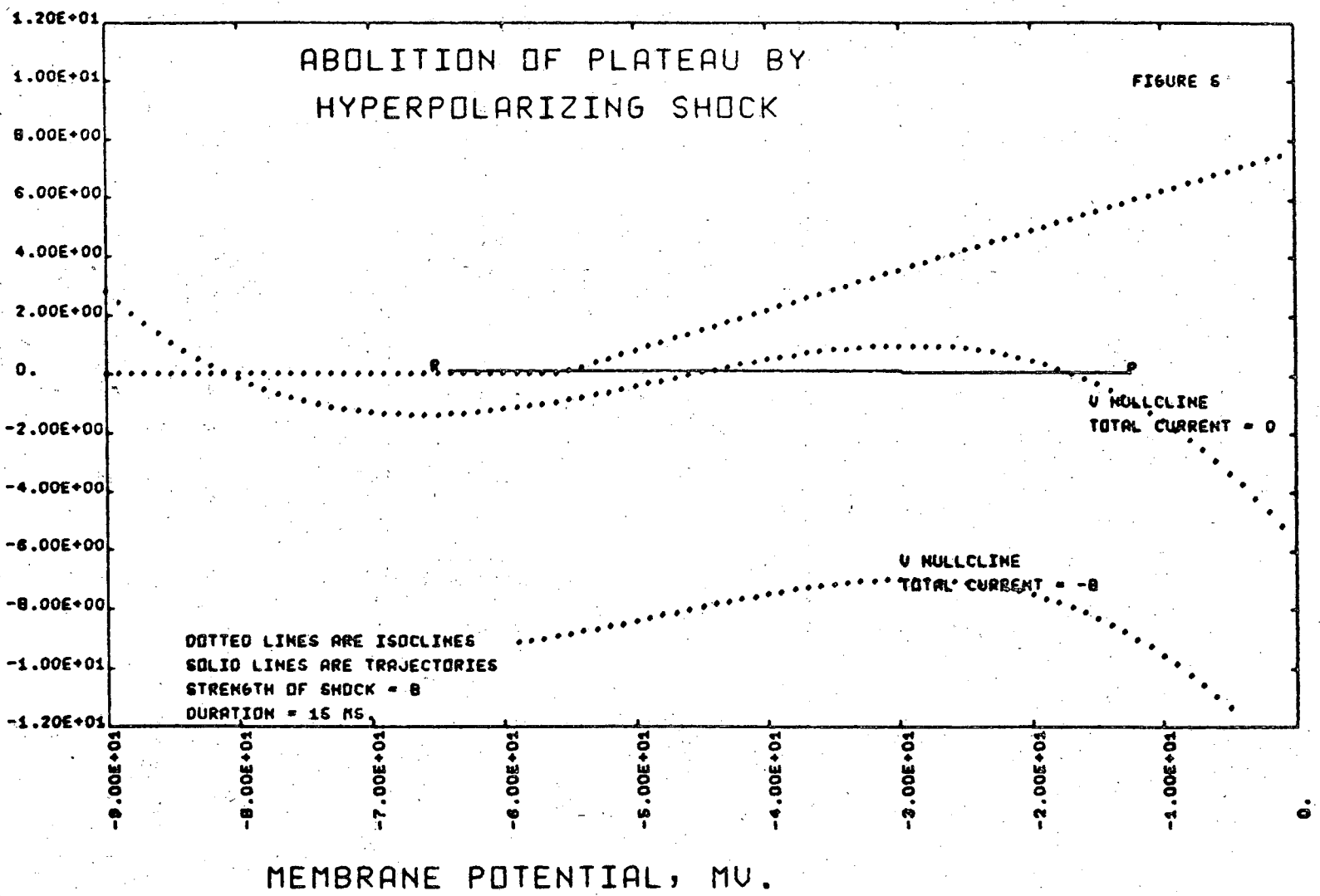
repolarization which would resemble qualitatively the strength-duration

curve for evocation of the action potential. Strong hyperpolarizing cur-

rents would cause $\frac{dV}{dt}$ to become strongly negative, and the phase point would

traverse the region between the V nullcline and the V axis in figure 4

more rapidly than it would in the case of a weaker hyperpolarizing current;

thus the weaker current would require more time in order to provoke abol-

ition of the plateau and repolarization to the resting potential. A sim-

ilar explanation of this phenomenon appears in (16).

2. Self-Excited Oscillations

For the purposes of the following analysis of the stability of the

system, let us rewrite (2.2) and (2.3) as follows:

$$i(V,W) = I(V) + W + C\frac{dV}{dt} \tag{2.4}$$

$$\frac{dW}{dt} = \alpha V - \beta W + \gamma, \quad V \geqslant -55$$

$$= -\beta W \quad , \quad V < -55$$

where $i(V,W)$ is the total membrane current, and α, β, and γ are constants

that arise as combinations of W_o and the parameters of x_∞ in the deriva-

tion of (2.4) from (2.2) and (2.3). (2.4) is in the form of the current

clamped case, i.e. that case where the time course of the current is pre-

determined; this corresponds to the case of a given current injected

through a microelectrode, among other things. Of course, propagation

effects will be neglected for the time being; thus (2.4) describes a

short fiber, or one that has been space clamped.

We shall examine the behavior of solutions to (2.4) by considering

the stability of the equilibrium points of the system for various constant values i_o of the total current $i(V,W)$. Physiologically this would represent a pathological steady leakage current or a steady current injected into a healthy cell through a microelectrode or across a sucrose gap. This is not the only way instabilities in (2.4) could be produced. It would be helpful to have some idea of the nature of the pathology of those fibers that exhibit the self excited oscillations spontaneously; any number of changes in the form of $I(V)$ could produce them, e.g. the opening of a channel with linear conductance and a reversal potential in the plateau range or below could change the phase portrait from one resembling figure 3 to one resembling figure 6. This could quite easily result in self excited oscillations, either spontaneously, or with the injection of a steady current. Now, for a given value of i_o, let (V^o, W^o) be an equilibrium point for (2.4). Then:

$$i_o + I(V^o) + W^o = 0$$
$$\alpha V^o - \beta W^o + \gamma = 0$$

(2.5)

We have also:

$$I(V) = I(V^o) + (V-V^o)I'(V^o) + \frac{1}{2}(V-V^o)^2 I''(V^o) + \ldots$$

Now putting $U = V-V^o$, $Y = W-W^o$, $a_1 = I'(V^o)$, $a_2 = \frac{1}{2}I''(V^o)$, $a_3 = \frac{1}{6}I'''(V^o)$

We arrive at:

$$C\frac{dU}{dt} = -a_1 U - a_2 U^2 - a_3 U^3 - Y$$

(2.6)

$$\frac{dY}{dt} = \alpha U - \beta Y$$

where we have explicitly made use of the fact that $I(V)$ is a cubic polynomial.

PHASE PORTRAIT FOR SYSTEM
WITH LINEAR CONDUCTANCE ADDED

FIGURE 6

RESTORING CURRENT, MICROAMPS/(SQ.CM)

MEMBRANE POTENTIAL, MV.

.80E+01

.60E+01

.40E+01

.20E+01

0.

-.20E+01

-.40E+01

-.60E+01

-.80E+01

SOLID LINES ARE ISOCLINES
DOTTED LINE REPRESENTS ADDED
LINEAR ELEMENT

-.90E+02
-.80E+02
-.70E+02
-.60E+02
-.50E+02
-.40E+02
-.30E+02
-.20E+02
-.10E+02

0.
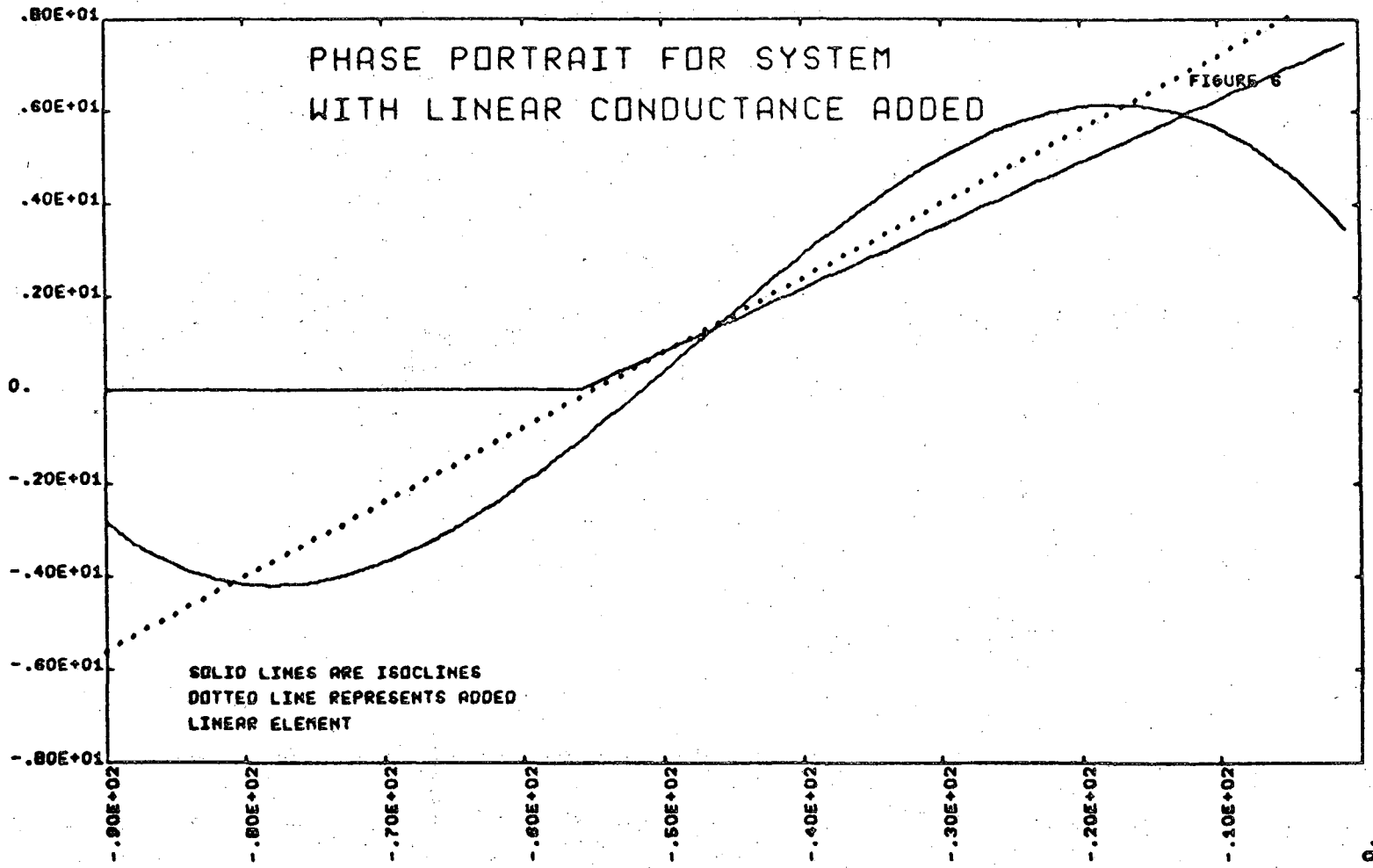
The linearized system in a neighborhood of (V^o, W^o) has the form:

$$\frac{d}{dt} \begin{pmatrix} U \\ Y \end{pmatrix} = \begin{pmatrix} \frac{-a_1}{C} & \frac{-1}{C} \\ \alpha & -\beta \end{pmatrix} \begin{pmatrix} U \\ Y \end{pmatrix} \tag{2.7}$$

We know from the classical theory of ordinary differential equations that the stability of the system (2.7) in a neighborhood of the origin, which corresponds to the stability of system (2.6) in a small neighborhood of (V^o, W^o), is characterized by the eigenvalues were computed numerically for integer values of V^o from -1 to -80, assuming $C = 3$, with the following results:

    V = -1 to V = -23mV   Eigenvalues real and negative

    V = -24 to V = -29   Eigenvalues conjugate complex, real part
                          negative

    V = -30   to   -35   Eigenvalues conjugate complex, real part
                          positive

    V = -36   to   -54   Eigenvalues real and positive

    V = -55   to   -66   Eigenvalues real and of opposite sign

    V = -67   to   -80   Eigenvalues real and negative.

In order to determine whether self-excited oscillations will occur for a given total current i_o, we compute the corresponding value of V^o, and then find the eigenvalues of the linearized system in a neighborhood of (V^o, W^o). It is interesting to note that while the value of C does not affect V^o (Note that W^o is linearly related to V^o), it does affect the eigenvalues of (2.7) and thus the stability of the equilibrium point (V^o, W^o).

The equilibrium potential V^O and the equilibrium restoring current W^O as functions of the total current i_o are given in figure 7. These points (V^O, W^O) are the intersections of the V and W nullclines on the phase portrait for the system with total membrane current i_o.

It is clear that all solutions of (2.6) stay bounded for all time. To see this, simply multiply the first equation by αU and the second by Y, and add the two resulting equations together. The result is an expression for $\frac{1}{2} \frac{d}{dt}(\alpha U^2 + Y^2)$ that is quartic in U and quadratic in Y with negative leading coefficients, from which it follows that the time derivative of $\alpha U^2 + Y^2$ will be negative for all U and Y sufficiently large in absolute value. Numerical evidence indicates that for equilibrium potentials in the plateau range (i.e. $\geq$ -48 mV or so) there is only one equilibrium point for the whole system; this corresponds to leakage currents greater than 1.5 $\mu A/cm^2$ or so, given a membrane capacitance of 1 $\mu F/cm^2$. We can see from (2.4) that membranes with larger capacitances require more current to displace the resting potential an equivalent amount. If there is a unique equilibrium point and the eigenvalues of the matrix in (2.7) have positive real part, then solutions starting near the equilibrium point must spiral outward and, staying bounded, must approach a limiting orbit which is necessarily periodic. This is the content of the well known Poincaré-Bendixson theorem (see, e.g., (13), pp. 109-111).

For some positive values of i_o there will be two or more critical points; this can be seen by taking the cubic curve in figure 3 and translating it upward without changing its shape. In these cases the possibility of other behavior arises. Numerical computation of approximate solutions to (2.4) in one of those cases with three equilibrium points

EQUILIBRIUM VALUES OF SYSTEM
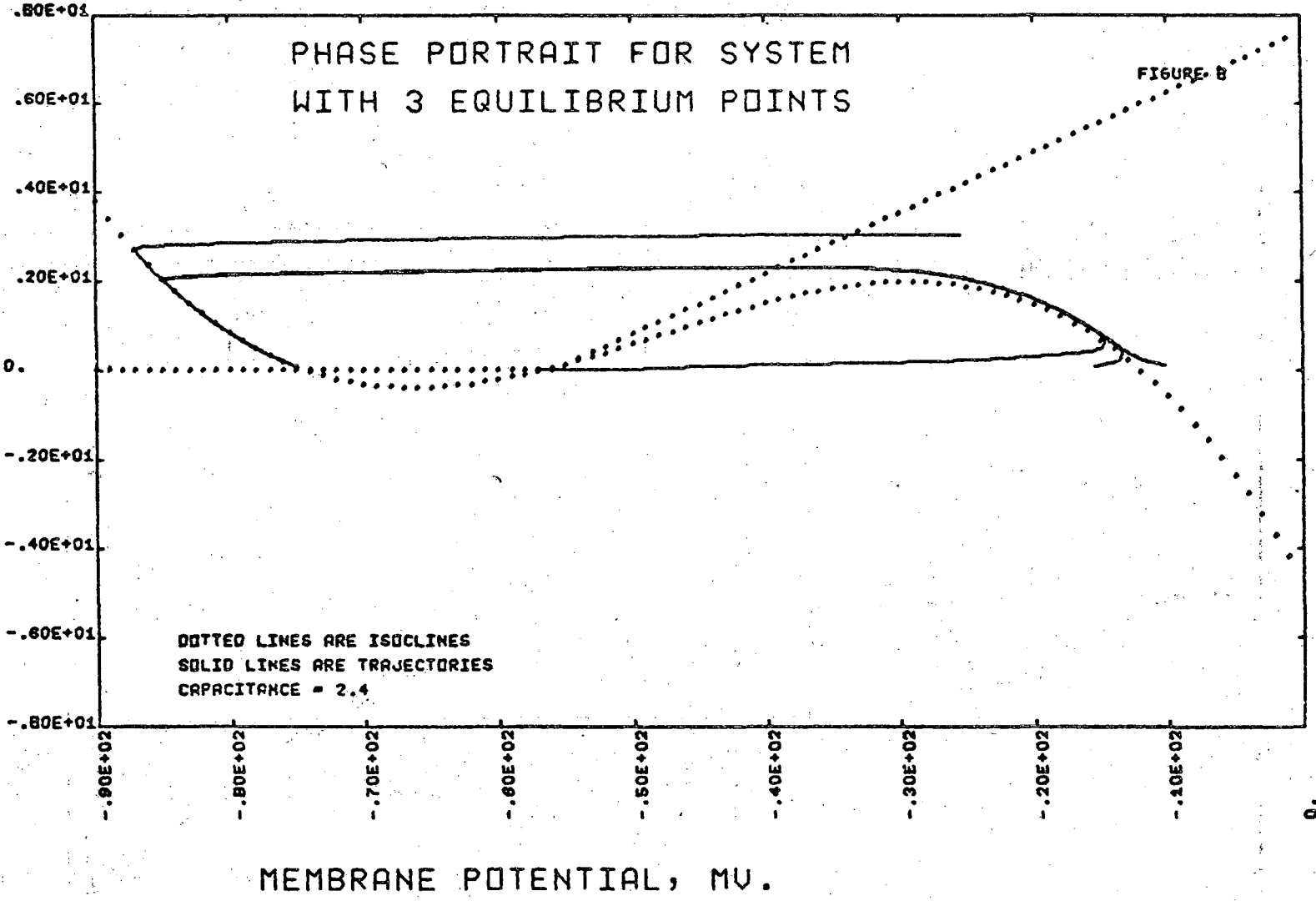
VERSUS TOTAL CURRENT

FIGURE 7
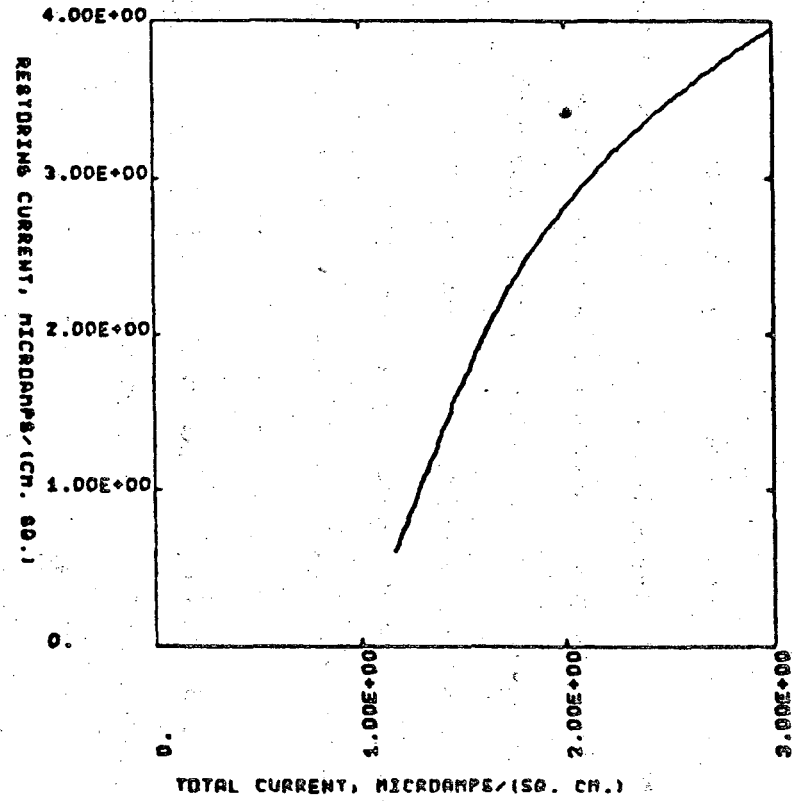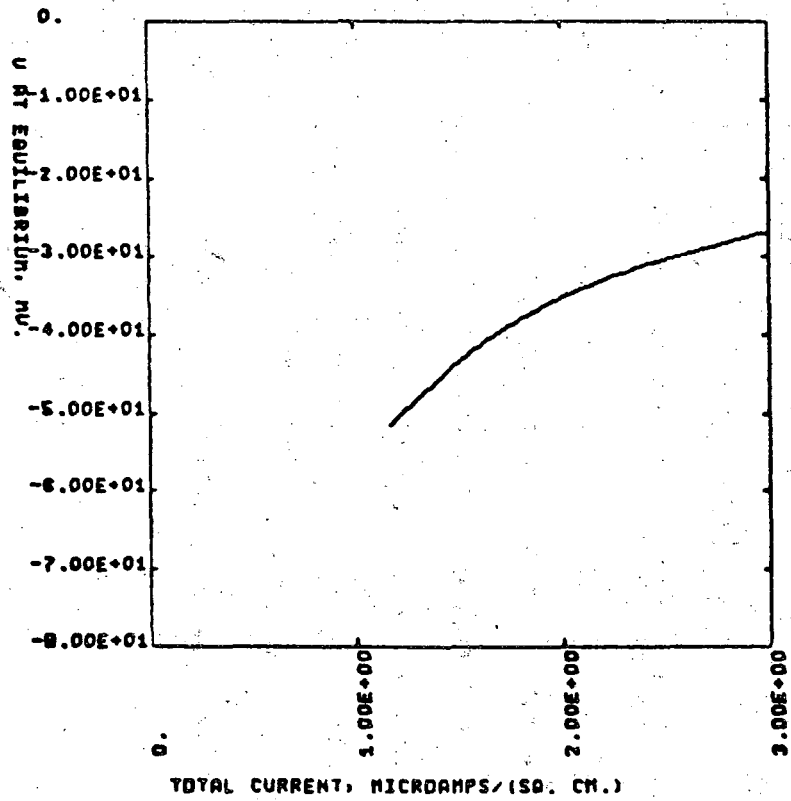
indicates that no new behavior worthy of additional consideration occurs.
The results of these computations are summarized in figure 8.

Let us turn now to the experimental data on the self-excited oscillations shown in figure A6. Given a typical area for these fibers of .005 cm^2 ((12), page 259), we may convert the currents shown in figure A6 to currents per unit area, and compare the experimental results to the predictions of the model. The results in figure A6 indicate that as the injected hyperpolarizing current passes through a range of approximately 2 microamps/cm^2, the fiber passes from stability at -20 millivolts through states of self-excited oscillation with increasing amplitude and period to a stable state near -50 millivolts, in good agreement with the model. We can see from figures 9, 10 and 11 that the statement on page 255 of (12) that "The amplitude and frequency of the oscillations are very sensitive to applied currents less than 1 microamp/cm^2. Larger currents abolish the oscillatory activity " also applies to our model. Thus in this model, as in the real system, equilibrium potentials between -30 and -50 millivolts are unstable, and oscillations results. Stable oscillations of realistic magnitude and period appear at leakage currents near 2.6 microamps/cm^2; for leakage currents slightly less than 2.6, the oscillations will be much slower, with magnitudes large enough to carry the potential out of the region of applicability of this simple model. Hence the oscillations in the plateau range observed by Hauswirth, Noble and Tsien in (12) are observed in the numerical solutions of the equations comprising this model. The agreement of our computational results with experiment lends support to the statement in the "Discussion" section of (12) that "...it should be relatively easy to induce low voltage oscillatory

PHASE PORTRAIT FOR SYSTEM
WITH 3 EQUILIBRIUM POINTS

FIGURE 8

DOTTED LINES ARE ISOCLINES
SOLID LINES ARE TRAJECTORIES
CAPACITANCE = 2.4

RESTORING CURRENT, MICROAMPS/(SQ.CM)

MEMBRANE POTENTIAL, MV.

MEMBRANE POTENTIAL OSCILLATIONS

FIGURE 9

•••• TOTAL CURRENT = 2.75
——— TOTAL CURRENT = 2.61
INITIAL POTENTIAL = -65

MEMBRANE POTENTIAL, MV.

TIME, MS.

MEMBRANE POTENTIAL OSCILLATIONS

FIGURE 10

MEMBRANE POTENTIAL OSCILLATIONS

MODULATION OF OSCILLATORY
ACTIVITY BY A SERIES OF
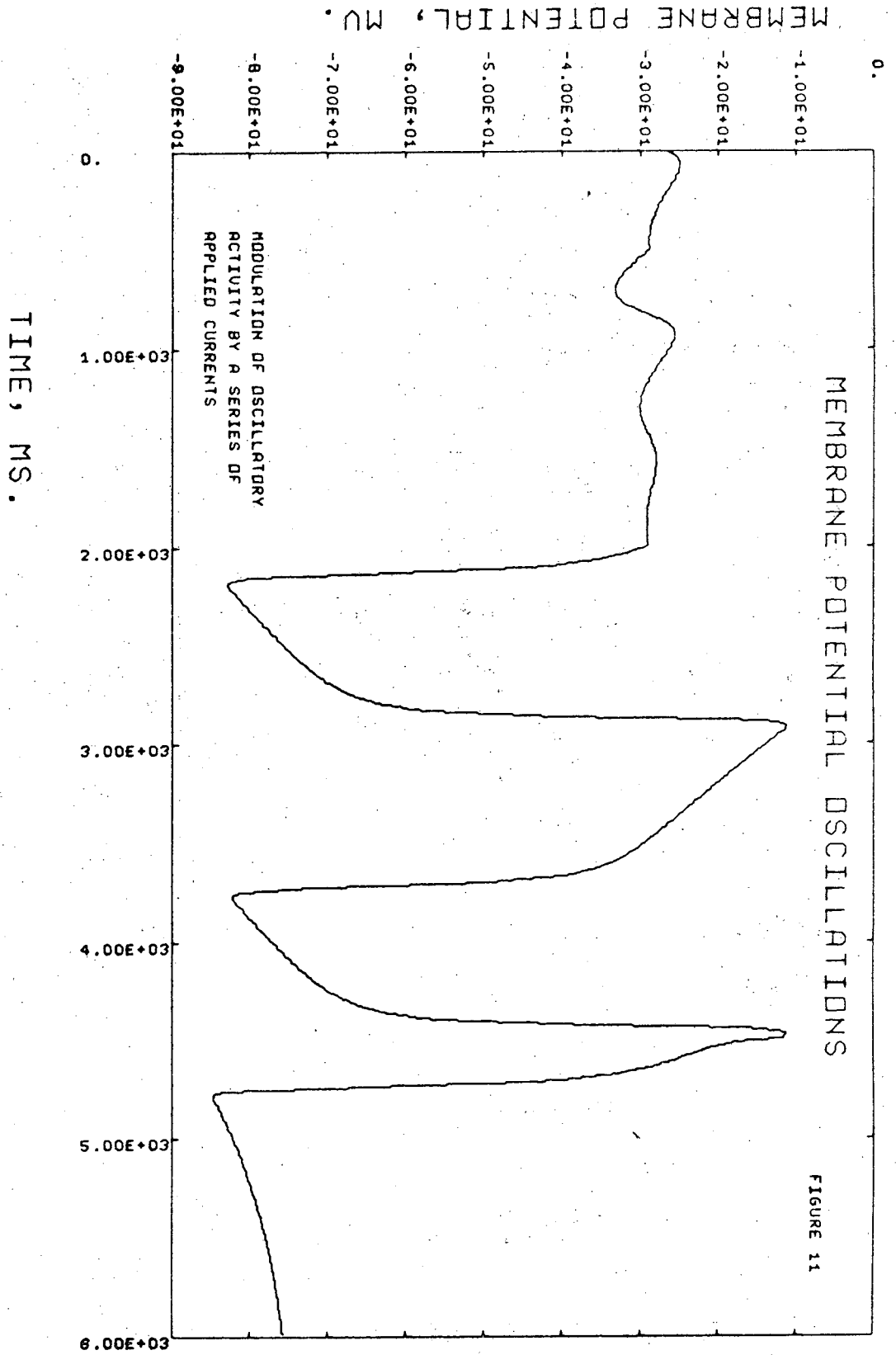APPLIED CURRENTS
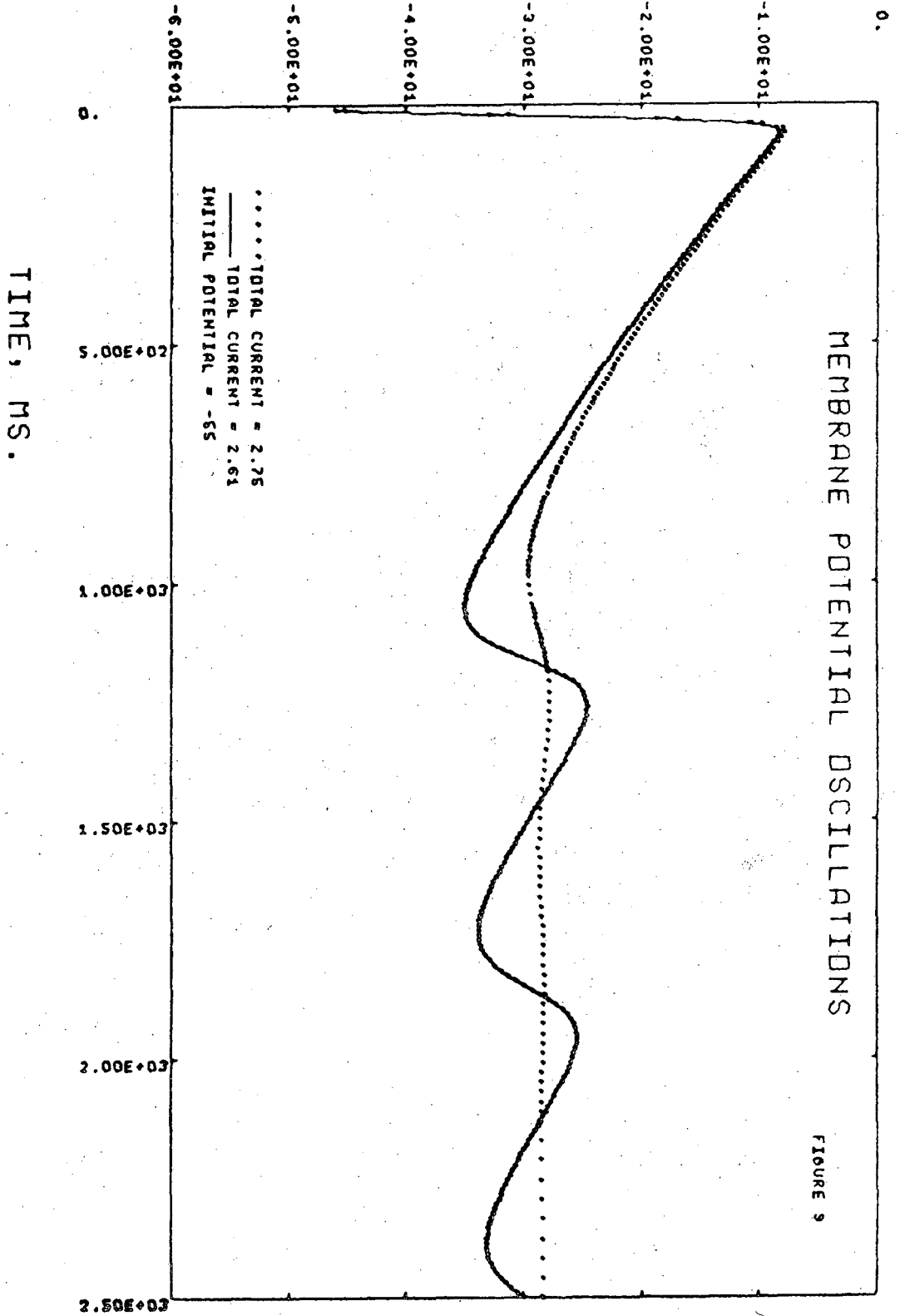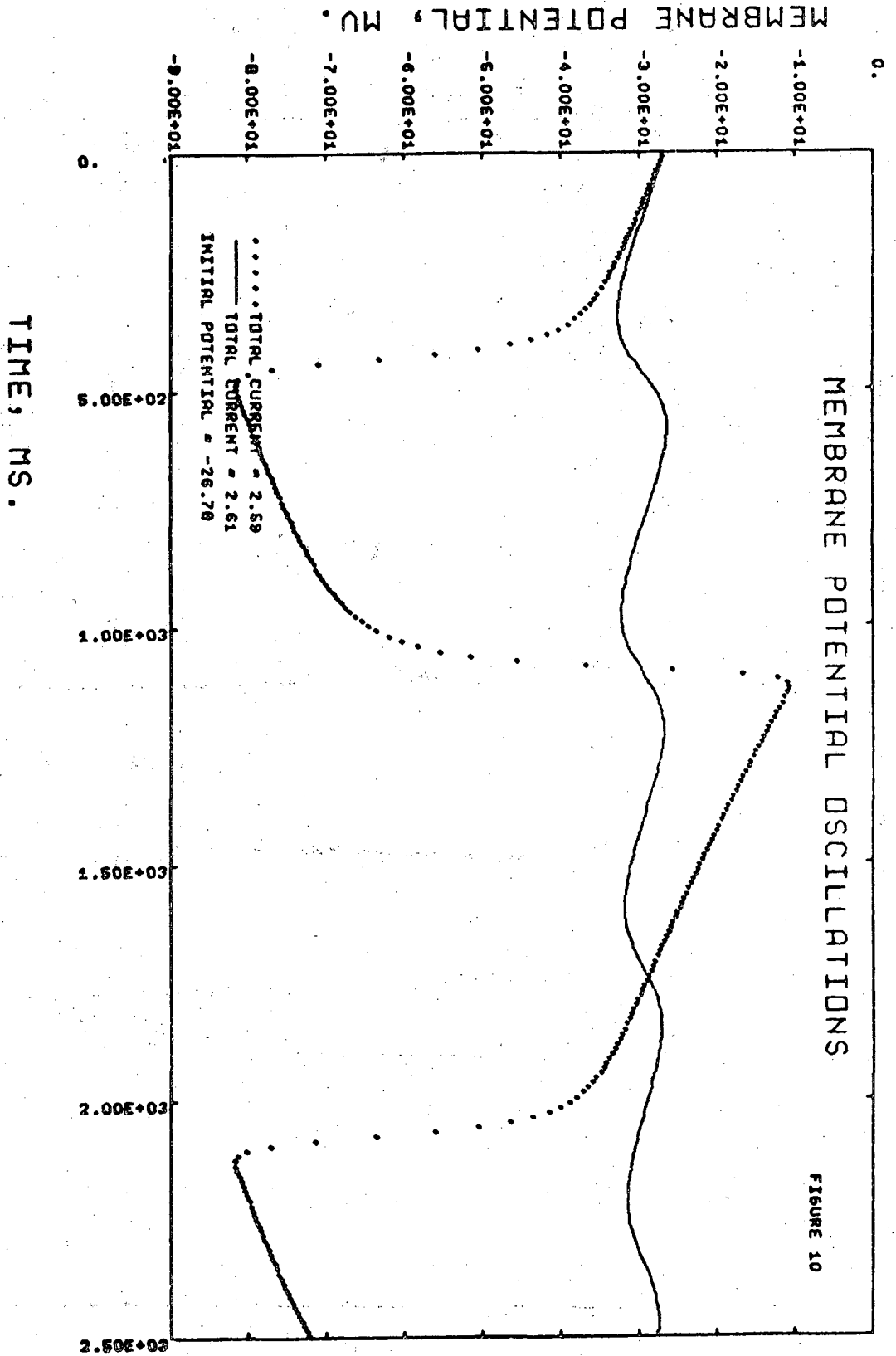
FIGURE 11

activity in normal preparations by procedures which simply vary the amount of background current...low voltage oscillations represent a mode of activity of relatively normal membranes."

3. A Model of the Purkinje Fiber Action Potential

We next construct a model that combines the plateau kinetics described above with Hodgkin-Huxley type sodium kinetics to produce simulated Purkinje fiber action potentials. No attempt was made to include the fast outward transient that is responsible for the notch observed at the beginning of the plateau (this notch is perceptible in figure A4 in the top and bottom traces; it is more pronounced in other records in the literature) and the pacemaker potential, which manifests itself as a slow depolarizing current in phase 4, and is responsible for spontaneous pacemaker activity in some Purkinje fibers.

Before presenting the model itself, let us review briefly the kinetics of the fast sodium current in the Hodgkin-Huxley model. The sodium current is assumed to be proportional to the difference between the membrane potential and the sodium equilibrium potential V_{Na} given by the Nernst equation:

$$V_{Na} = \frac{RT}{F} \ln \frac{[Na]_{external}}{[Na]_{internal}}$$

where T is the absolute temperature, R is the universal gas constant, F is the charge in coulombs of a mole of elementary charges, and square brackets denote concentration. The factor of proportionality, i.e. the conductance, depends on two dimensionless parameters m and h which vary between zero and one. The parameters m and h obey first order rate equations whose coefficients depend on the membrane potential V. We introduce

for m the rate constants α_m and β_m, both depending on V as follows:

$$\alpha_m(V) = 0.1(V + 25)[\exp((V + 25)/10)-1]^{-1}; \quad \beta_m = 4\exp(V/18) \qquad (2.8)$$

and similarly for h:

$$\alpha_h(V) = .07\exp(V/20); \quad \beta_h(V) = (\exp[(V + 30)/10] + 1)^{-1} \qquad (2.9)$$

We may now write the rate equations for m and h:

$$\frac{dh}{dt} = \alpha_h(V)(1-h)-\beta_h(V)h \qquad (2.10)$$

$$\frac{dm}{dt} = \alpha_m(1-m)-\beta_m m$$

In terms of m and h, we write the sodium conductance as:

$$g_{Na} = m^3 h \bar{g}_{Na}$$

where $\bar{g}_{Na}$ is the peak sodium conductance. The effect of temperature may be simulated by multiplying the right hand side of equations (2.10) by some function of temperature ϕ. (for details, see (7), page 25; for further modifications, see (8)).

To gain some insight into the behavior of m and h, let us define four new functions of V; m_∞, τ_m, h_∞, τ_h as follows:

$$m_\infty = \frac{\alpha_m}{\alpha_m + \beta_m}; \quad \tau_m = \frac{1}{\alpha_m + \beta_m}$$

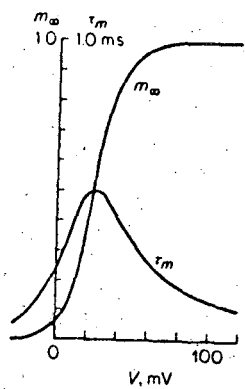Steady State Values of m and h as Functions of Potential
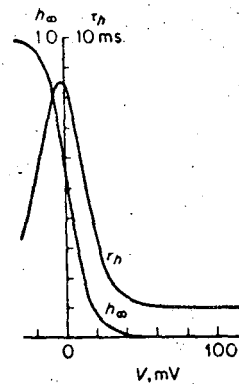

Figure 12

Figure 13

From page 25 of (7)

and likewise for h. (2.10) then become:

$$\frac{dm}{dt} = \frac{m_\infty - m}{\tau_m} \; ; \; \frac{dh}{dt} = \frac{h_\infty - h}{\tau_h}$$

Thus if V is held constant, m decays to m_∞ with time constant τ_m, and h decays to h_∞ with time constant τ_h. m_∞, τ_m, h_∞ and τ_h are very complicated functions of V, but an intuition can be gained for the behavior of (2.11) by examining their graphs which are displayed in figures 12 and 13. The whole expression for the sodium current in this model is:

$$i_{Na} = \bar{g}_{Na} m^3 h (V - V_{Na}) \qquad\qquad (2.12)$$

Under normal conditions, V_{Na} is approximately 120 mV., so the i_{Na} term is negative at rest, but very small in magnitude due to the small value of m near the resting potential.

Let us now examine the behavior of the sodium current during phase 1 as illustrated in figure 14. Suppose the system starts in equilibrium, and is subjected at time t = 0 to a short pulse of inward current that quickly raises the membrane potential V from rest by 20 to 40 millivolts. The value of m_∞ at this new potential is near .5, while the value of h_∞ at the new potential is very nearly zero. Since τ_m is very much less than τ_h, m approaches its new equilibrium value rapidly, while h remains near its original value for some time. Since the new equilibrium value of m and the original (i.e. evaluated at resting potential; see figure 13) equilibrium value of h are comparatively large, the total sodium current

Computed Time Course of Potential and Conductance Parameters m and h

for the Hodgkin-Huxley Model

Figure 14

-29-
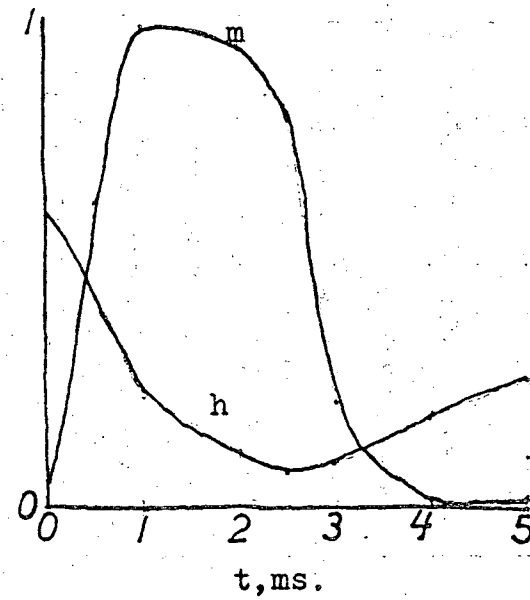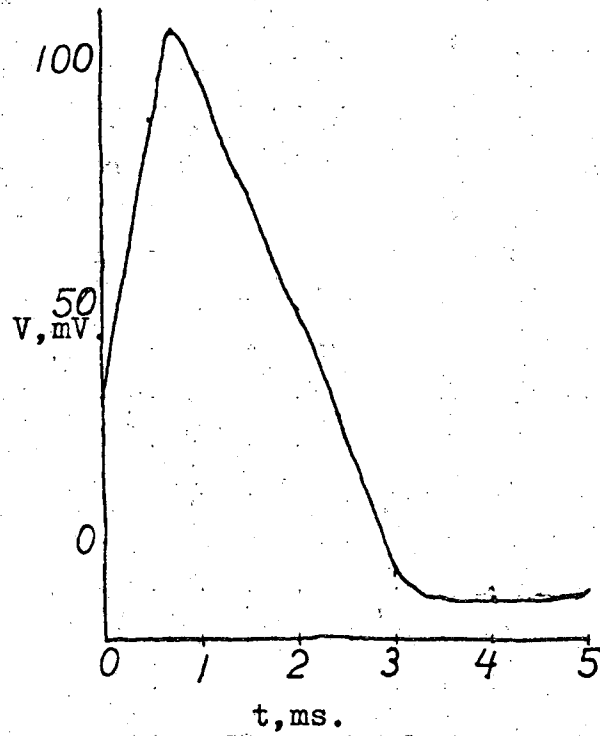
becomes very strongly negative for a short time (i.e. $<<\tau_h$). Since the total current is the sum of the ionic current and the capacity current (given by $C\frac{dV}{dt}$) and the other components of the ionic current remain very nearly constant over times comparable to τ_m, $\frac{dV}{dt}$ must become positive under current clamp conditions. The result is illustrated as phase 1 in figure 14. As phase 1 continues and V rises, we note from the lower graph in figure 14 that m rises with it, while h does not reach its minimum until well into phase 3. Phase 1 ends as the rise in V is limited by two factors: as V approaches V_{Na}, the total sodium current (given in (2.12) decreases; and eventually, h begins to decrease sharply, since its equilibrium value at potentials greater than 60 mV above resting potential is effectively zero, as shown in figure 13.

We have noted above that the assumptions underlying the derivation of (2.1) break down outside of the plateau region, and extension of the model to more positive or negative potentials requires the introduction of nonconstant functions of V for τ and W_o, and the modification of $x_\infty(V)$ so that it will take a constant value of 1 at potentials greater than a given cutoff potential. We choose this cutoff potential by requiring that x_∞ be continuous, i.e. we solve 2.2 for the value of V such that $x_\infty = 1$, and set $x_\infty \equiv 1$ for all larger V. By this process we find the cutoff to be V = 3.0088 mV. W_o was fitted to Noble and Tsien's experimental data (fig. A3) by a quadratic polynomial and τ^{-1} is fitted to figure A1 by a least squares cubic. The explicit forms of these polynomials are given below:

$$W_o = -1.983 \times 10^{-3}(V - 50)(V + 80.73)$$

$$\tag{2.13}$$

$$\tau^{-1} = 2.365 + .009141\ V - 3.582 \times 10^{-4}\ V^2 - 9.166 \times 10^{-6}\ V^3$$

The integrated model is essentially a combination of 2.1 with W_o and τ as in (2.13) with excitation modeled (by 2.12). One last step in the construction remains: I(V) implicitly contains the steady state sodium current, since the experiments on which its construction is based involve time scales so much longer than τ_m that the sodium kinetics are regarded as occurring instantaneously. Therefore a term of the form $\bar{g}_{Na}m_\infty^3 h_\infty(V-V_{Na})$ must be subtracted from the sum of the sodium current and the plateau currents to avoid counting the steady state sodium current twice.

We now have all the terms necessary to write down equations that will model the behavior of a fiber with Hodgkin-Huxley excitability and a plateau with the kinetics observed by Noble and Tsien for Purkinje fibers(16) The equations are:

$$i(V,x,m,h) = C\frac{dV}{dt} + I(V) + W + \bar{g}_{Na}m^3h(V - V_{Na}) - \bar{g}_{Na}m_\infty^3 h_\infty(V - V_{Na})$$

$$W = xW_o(V)$$

$$\frac{dx}{dt} = \tau^{-1}(V)(x_\infty(V) - x)$$

$$\frac{dm}{dt} = \frac{m_\infty - m}{\tau_m}$$

$$\frac{dh}{dt} = \frac{h_\infty - h}{\tau_h}$$

(2.14)

It would seem from the vastly different time scales of the upstroke of the action potential and the plateau that problems of stiffness would arise in any numerical calculation associated with a model of the Purkinje fiber action potential. Such stiffness problems do indeed await the unwary user of explicit methods with long time steps, especially if he attempts to lengthen his time steps by using highly accurate multistep methods.

The failure of such tactics is well illustrated in figure A7. This graph is reproduced from (15), which is a study of numerical techniques for the Hodgkin-Huxley system. If an implicit method is used, one may take time steps of the same order as the slowest time constant in the problem once the fast parameters have come sufficiently close to their equilibrium values that further details of their time courses are no longer of interest. Thus, if an implicit method were used to integrate (2.14), we could expect to take time steps of the same order as the times characteristic of the plateau once the sodium transient decayed. However, the added complication of the implicit methods adds so much computational overhead that the longer time steps they take may not result in any overall saving in computing cost over explicit methods unless the stiffness of the system is quite pronounced. For (2.14), Huen's second order explicit Runge-Kutta method was observed to perform as well as Miller's second order diagonally implicit Runge-Kutta method which is specifically designed to deal with stiff systems (see K. Miller (14) for details of this method and stiff systems in general). The damping effect of h upon m seems to stabilize the system and eliminate much of the stiffness after the fast transients have died out. The usual stepsize changing algorithm allowed Huen's method to take time steps as long as the longest allowed by the diagonally implicit Runge-Kutta method. However, future investigators would probably do well to keep in mind the fact that because of their essential dependence on widely differing time constants, Hodgkin-Huxley type systems are inherently stiff, and in some cases may require specialized methods for practical computation.

A typical action potential computed from equations (2.14) is

illustrated in figure 15. A system of partial differential equations could be derived from (2.14) in order to model the behavior of propagated impulses in Purkinje fibers. Unfortunately this is not a computationally practical model because a fine space grid is required to resolve the quasi-threshold behavior of the sodium current. This limitation, combined with the excessively small time constants of the upstroke relative to the long time constants of the plateau (i.e. stiffness, or greatly differing time constants) leads to excessive computational expense, even on a computer with the speed and cost effectiveness of the CDC 7600.

We should note finally that this model contains the implicit assumption that the instantaneous current-voltage relation $I(V)$ is actually instantaneous; this assumption was warranted for the modeling of the plateau with its long time scales but since this integrated model is intended to deal with time scales of the same order as the sodium activation time, the assumption is no longer consistent.

The next sections deal with a qualitative partial differential equation model which will be used to investigate the nonlinear propagation phenomena observed in (4).

PURKINJE FIBER ACTION POTENTIAL

FIGURE 15
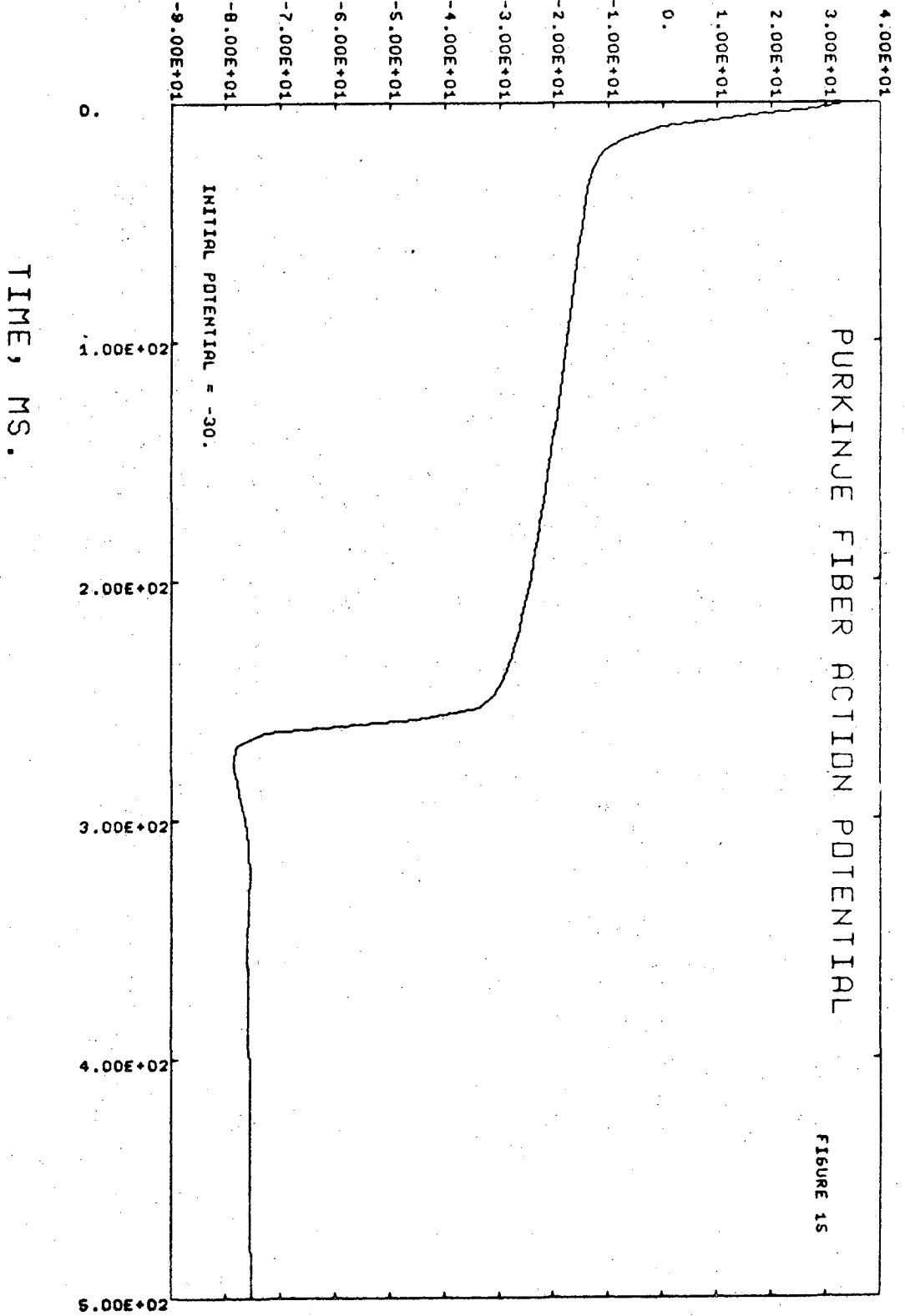
III. THE SIMPLIFIED MODEL

1. O.D.E.'s for the Space Clamped Case

In this and the following sections the purely qualitative model re-
ferred to in the introduction will be described, as well as the numerical
schemes used to compute results from it and the numerical results them-
selves. We shall begin our discussion with a presentation of the ordinary
differential equations that describe the space clamped case, or equiva-
lently, a small patch of membrane in which there is no appreciable spatial
variation in potential.

For the purposes of the following analysis, a homogeneous patch of
membrane will be considered as a parallel RC network in parallel with a
nonlinear conductor, which may be represented schematically as follows:

Figure 16

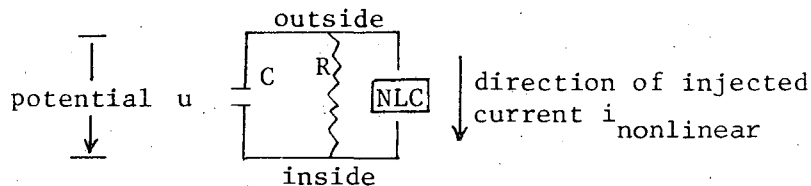where the rectangle labeled NLC is a nonlinear conductor with properties
as follows: for $u <$ some constant voltage a, it acts as an open circuit;
for $u \geqslant a$, a current is injected in the direction indicated which decays
exponentially in time with time constant τ_h. We write this as follows:

$$i_{nonlinear} = \begin{cases} 0, & u < a \\ \dfrac{E_o h}{R}, & u \geqslant a \end{cases}$$

(3.1)

where h is a dimensionless variable which takes on values between 0 and

1 according to the following O.D.E.:

$$\frac{dh}{dt} = \frac{1 - H(u - a) - h}{\tau_h} \qquad (3.2)$$

E_o and τ_h in the above two equations are constants with the dimensions

of potential and time respectively; $H(y)$ is the Heaviside function, i.e.

$H(y) = 0$ if y is negative and 1 if $y \geqslant 0$.

If we write:

$$RC = \tau$$

and set the sum of the currents in the resistor, capacitor and NLC equal

to zero, we arrive at the following differential equations or the behavior

of the circuit in fig. 16:

$$\frac{du}{dt} + \frac{1}{\tau}u = \frac{E_o}{\tau} H(u - a)h$$

$$\qquad (3.3)$$

$$\frac{dh}{dt} = \frac{1 - H(u-a) - h}{\tau_h}$$

At rest, $u = 0$ and $h = 1$. If, however, the model is brought to

threshold, say by a stimulating current appearing as a positive term on

the right hand side of the first equation of (3.3), the solution may be

found as follows: Let us begin at $t = 0$ with $u = a$ and $h = 1$. Then

$H(u-a) = 1$, and so, for a short time at least, $h = \exp(-t/\tau_h)$, assuming

E_o is large enough to make $\frac{du}{dt}$ positive when $u = a$. The first equation of

(3.3) then becomes:

$$\frac{du}{dt} + \frac{1}{\tau} u = \frac{E_o}{\tau} \exp(-t/\tau_h)$$

Multiplying through by $\exp(t/\tau)$ yields:

$$\frac{d}{dt} [\exp(t/\tau)u] = \frac{E_o}{\tau} \left[\exp([\frac{1}{\tau} - \frac{1}{\tau_h}] t) \right]$$

integration with respect to to yields:

$$\exp(t/\tau)u(t) - u(0) = \frac{E_o \left(\exp\left[(\frac{1}{\tau} - \frac{1}{\tau_h}) - 1 \right] \right)}{\tau [\frac{1}{\tau} - \frac{1}{\tau_h}]}$$

So:

$$u(t) = u(0)\exp(-t/\tau) + \frac{E_o \left(\exp(-t/\tau_h) - \exp(-t/\tau) \right)}{1 - (\tau/\tau_h)} \qquad (3.4)$$

There are two limiting cases that are of interest: $\frac{\tau}{\tau_h} \to 0$ and $\frac{\tau}{\tau_h} \to \infty$. The first is the more realistic case from the point of view of the task of modeling of action potentials, but the second will lead to a P.D.E. with peculiar and interesting properties.

First, put $\frac{\tau}{\tau_h} = \epsilon \ll 1$. Then write:

$$s = t/\tau; \quad u(t) = v(s)$$

Substitution into (3.4) yields

$$v(s) = v(0)\exp(-s) + \frac{E_o}{1-\epsilon} (\exp(-\epsilon s) - \exp(-s)) \qquad (3.5)$$

So for short time, i.e., $s \ll 1/\varepsilon$, we have:

$$v(s) \approx v(0)\exp(-s) + E_o(1-\exp(-s)).$$

Graphically, this looks like:
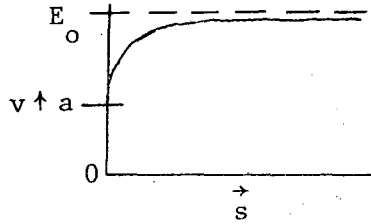
Figure 17

For time scales on the order of τ_h, the time scale of the decay of $i_{nonlinear}$, we introduce the variables $r = t/\tau_h$ and $w(r) = u(t)$. From (3.4) we find that:

$$w(r) = w(0)\exp(-r/\varepsilon) + \frac{E_o}{1-\varepsilon}(\exp(-r)-\exp(-r/\varepsilon))$$

$$\approx E_o\exp(-r)$$

(3.6)

as long as $w(r) \geqslant a$; when $w(r)$ decays to a, the current injected by the nonlinear element turns off, and the second term on the right hand side of (3.6) vanishes. Thus, to lowest order, $w(r)$ vanishes after this point, and the lowest order solution exhibits a jump from a to 0. This jump is actually an exponential decay with time constant ε in this time scale. We may determine the pulse length t_p to lowest order by setting:

$$E_o\exp(-r_p) \cong E_o\exp(-t_p/\tau_h) = a.$$

Dividing through by E_o and taking logs on both sides yields:

$$t_p = \tau_h \log\left(\frac{E_o}{a}\right)$$

By the foregoing, the complete solution must look like

Figure 18
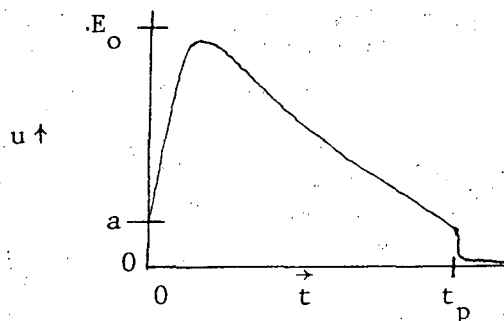
We note here that the above results could have been obtained by intro-ducing the scaled variables r and s into equations (3.3), solving the resulting systems to lowest order in ε, and then matching the solutions obtained, rather than writing down (3.4), the solution to (3.3), and examining the behavior of the solution for long and short times as we have done.

Let us turn now to the case $\tau/\tau_h \to \infty$. Actually, the case we will con-sider is not simply this limit, but the case in which $\tau/\tau_h \to \infty$ while the total charge injected by the nonlinear element remains constant. If this constant charge provision or something like it were not assumed, and all other parameters were held constant, then this case would reduce to that of a current injected for a decreasing amount of time, which would become trivial in the limit.

to see this, let us consider the total charge injected by the non-linear element if the potential is maintained above threshold for infinite time. The total charge Q is given by:

$$Q = -\int_0^\infty i_{nonlinear} dt = -\int_0^\infty \frac{E_o C}{\tau} \exp(-t/\tau_h) dt$$

$$= \frac{-\tau_h}{\tau} CE_o \exp(-t/\tau_h)\Big|_{t=0}^\infty = \frac{\tau_h}{\tau} E_o C$$

(3.7)

So the capacity of the membrane will be charged to a potential of

$\frac{Q}{C} = \frac{\tau_h}{\tau}(E_o)$ which vanishes as τ_h/τ goes to zero. Let us rewrite (3.3) so

that Q remains constant as follows:

$$\frac{du}{dt} + \frac{1}{\tau}u = \frac{Q}{C\tau_h} H(u-a)h$$

$$\frac{dh}{dt} = \frac{1 - H(u-a) - h}{\tau_h}$$

(3.8)

(3.4) then becomes:

$$u(t) = u(0)\exp(-t/\tau) + \frac{Q}{C(1-\varepsilon)} \exp(-t/\tau)-\exp(-t/\tau_h) \qquad (3.9)$$

where $\varepsilon = \tau_h/\tau$. As $\varepsilon \to 0$, this model reduces to a model devised by Charles

Peskin in which the nonlinear element in fig. (16) injects a delta-function

of current when the potential passes a certain threshold. We may now

repeat the analysis given above to determine the behavior of solutions to

(3.8) for small ε. Writing $r = t/\tau_h$ and $v(r) = u(t)$, we find

$$v(r) = v(0)\exp(-\varepsilon r) + \frac{Q}{C(1-\varepsilon)} [\exp(-\varepsilon r) - \exp(-r)]$$

For short times, i.e. small values of r, the above reduces to

$$v(r) = v(0) + \frac{Q}{C} [1 - \exp(-r)]$$

For longer times of the order of τ, we choose the new time scale $s = t/\tau$,

and the new solution function $w(s) = u(t)$. Equation (3.9) then becomes:

$$w(s) = w(0)\exp(-s) + \frac{Q}{C(1-\varepsilon)} [\exp(-s)-\exp(-s/\varepsilon)]$$

which reduces to:

$$w(s) \approx [w(0) + \frac{Q}{c}]\exp(-s)$$

to lowest order.

Hence the solutions to the above O.D.E's are very similar in form for both of the limiting cases considered. We shall see, however, that these two cases behave very differently when we pass to the case of the partial differential equation describing a long fiber.

In order to compare this simple model with the more detailed model of the Purkinje fiber plateau presented in chapter II, we define a new parameter $p = 1 - h$, and write (3.3) as

$$\frac{du}{dt} = -\frac{1}{\tau}u + \frac{E_o}{\tau}(1-p)H(u-a)$$

$$\frac{dp}{dt} = \frac{H(u-a) - p}{\tau_h}$$

(3.10)

The phase portrait of (3.9) is given in figure 19. To the left of the vertical line $u = a$, this is exactly the phase portrait of Young's model, as illustrated in fig. 2.1 of (7), with the vertical line $u = a$ corresponding exactly to what FitzHugh calls the excitation barrier. To the right of the excitation barrier, the similarity to figure 3 is clear. In the plateau region, the simplified model can be expected to behave much like the more detailed model with small leakage current. The simple model will exhibit all or none repolarization from the plateau by exactly the same dynamics as the more detailed model.

The simple model will not reproduce the self excited oscillations that occur in nature and are exhibited by the detailed model. This failure results from the sharp discontinuity of H. If we were to replace H with some approximation H_z, for example, $H_z(x) = \dfrac{1}{1 + e^{-(x/z)}}$, and substitute

H_z for some small z in place of H in (3.10), the phase portrait of the new

system would resemble figure 20, in which self-excited oscillations could

quite plausibly occur.

2. Traveling Wave Analysis for the Partial Differential Equation

The PDE that describes the electrical behavior of a long fiber whose

space-clamped behavior is given in (3.3) above is:

$$\lambda^2 u_{xx} = \tau u_t + E_o H(u-a)h + u$$

$$h_t = \frac{1 - H(u-a) - h}{\tau_h}$$

$$(3.11)$$

where λ = the length constant of the membrane, and the subscripts x and t

represent differentiation with respect to length and time respectively.

E_o, τ, and τ_h are the same constants defined above in section 1 of this

chapter, i.e. E_o/R is the peak amplitude of the current injected by the

nonlinear conductor, τ is the passive membrane time constant and τ_h is

the time constant associated with the parameter h.

Let us scale the equation as follows:

$$y = \frac{x}{\lambda} ; \qquad s = \frac{t}{\tau}$$

(3.11) then becomes

$$u_{yy} = u_s + u - E_o H(u-a)h$$

$$h_s = \frac{\tau}{\tau_h} [1 - H(u-a) - h]$$

$$(3.12)$$

-43-

Figure 19

Phase Portrait of Simple Model
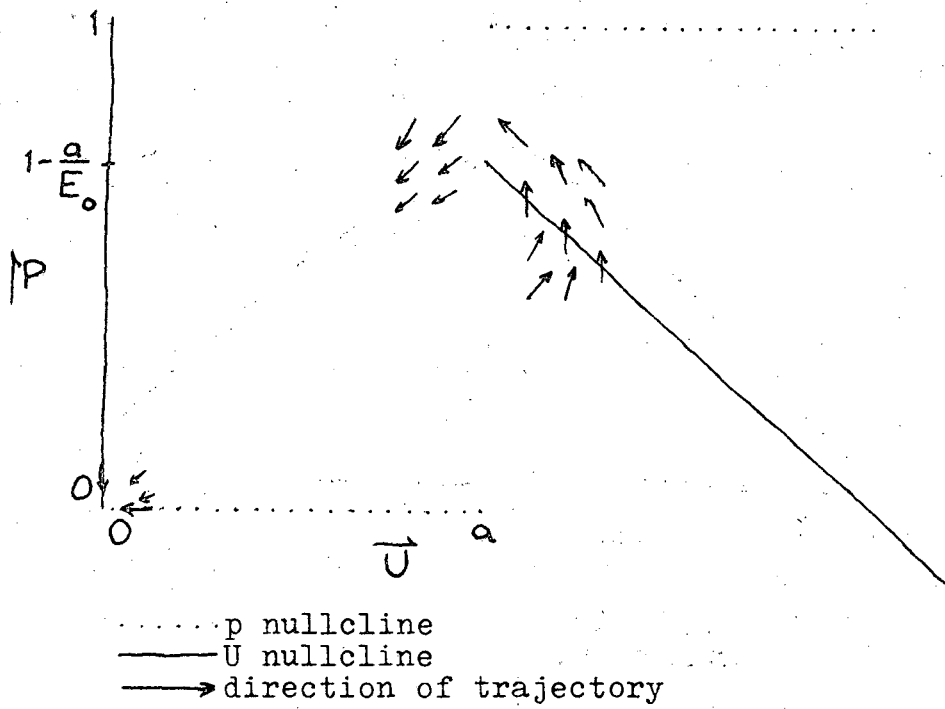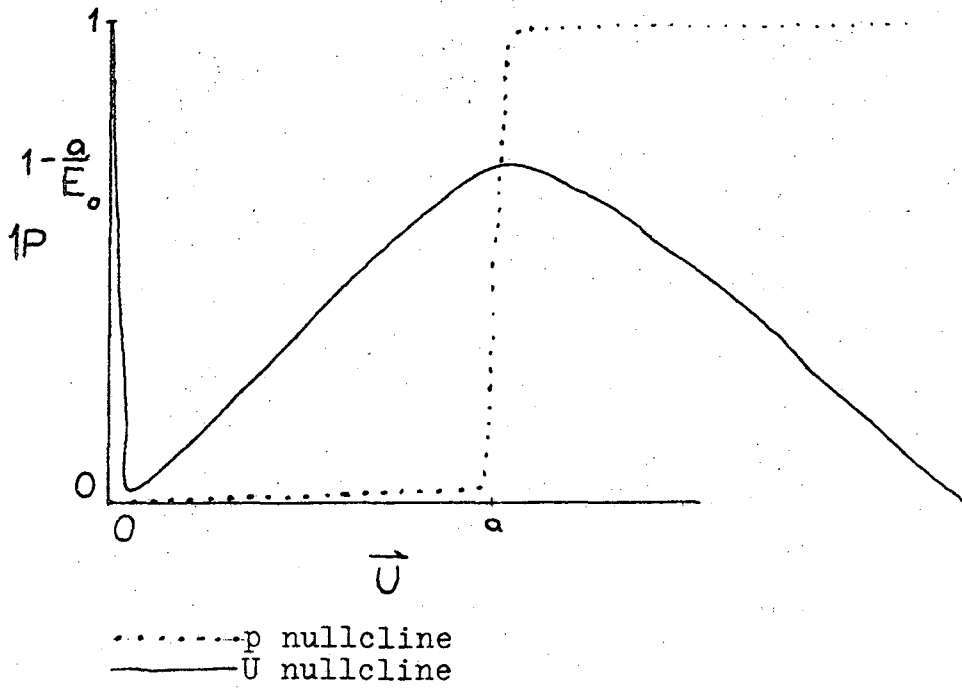

$$1$$

$$1-\frac{a}{E_o}$$

P

O

O

$\vec{U}$

a

······ p nullcline
——— U nullcline
———→ direction of trajectory

Figure 20

Phase Portrait of System with Pointwise
Approximate Step Function

$\cdots\cdots$p nullcline
———U nullcline

Now let us look for traveling wave solutions to (3.12) by transforming to a moving frame of reference translating to the left with speed θ. We do this by writing:

$$z = \frac{y}{\theta} + s$$

and seeking solutions of the form $u(y,s) = v(z)$ and $h(y,s) = h(z)$. The new functions v and h must satisfy the ordinary differential equations:

$$v'' = \theta^2 v' + \theta^2 v - \theta^2 E_o H(v-a)h$$

$$h' = \frac{\tau}{\tau_h} [1 - H(v-a)-h]$$

$$(3.13)$$

We now impose the following conditions on v:

$$v(0) = a; \quad v(z) \to 0 \text{ as } |z| \to \infty; \quad v \in c'(\mathfrak{R}); \quad v(z_1) = a \text{ for some } z_1 > 0 \qquad (3.13a)$$

We solve (3.13) subject to (3.13a) as follows: for $z \leqslant 0$, $h = 1$ and $v(z) = a\exp(\gamma_{\pm}z)$, where $\gamma_{\pm}$ are the roots of:

$$\gamma^2 - \theta^2\gamma - \theta^2 = 0, \text{ i.e. } \gamma_{\pm} = \frac{\theta^2 \pm \sqrt{\theta^4 + 4\theta^2}}{2} = \frac{\theta^2}{2}\left\{ 1 \pm \sqrt{1 + \frac{4}{\theta^2}} \right\}$$

Let us now consider the first limiting case discussed in section 1, i.e. $\frac{\tau}{\tau_h} = \epsilon \ll 1$. In the interval $0 \leqslant z \leqslant z_1$, $h = \exp(-\epsilon z)$, so in this region, (3.13) becomes

$$v'' = \theta^2 v' + \theta^2 v - \theta^2 E_o \exp(-\varepsilon z). \qquad (3.14)$$

It is then natural to look for solutions of the form:

$$v = A_1 \exp(\gamma_+ z) + A_2 \exp(\gamma_- z) + B \exp(-\varepsilon z) \qquad (3.15)$$

B is determined by substituting $B\exp(-\varepsilon z)$ into (3.14) which yields:

$$(\varepsilon^2 + \theta^2 \varepsilon - \theta^2)B = -\theta^2 E_o,$$

hence

$$B = \frac{-\theta^2 E}{\varepsilon^2 + \theta^2 \varepsilon - \theta^2}$$

Note here that $B \to E_o$ as $\varepsilon \to 0$.

The solution in the region $0 \leqslant z \leqslant z_1$ is given by (3.15) and the solution in the region $z > z_1$ is $v(z) = a\exp[\gamma_-(z-z_1)]$, $h = \exp[-\varepsilon(z_1+z)] + 1-\exp(-\varepsilon z)$. The condition that $v \in C^1(\Re)$ then becomes:

$$B + A_1 + A_2 = a$$

$$-\varepsilon B + \gamma_+ A_1 + \gamma_- A_2 = \gamma_+ a$$

$$\qquad (3.16)$$

$$B\exp(-\varepsilon z_1) + A_1 \exp(\gamma_+ z_1) + A_2 \exp(\gamma_- z_1) = a$$

$$-\varepsilon B\exp(-\varepsilon z_1) + \gamma_+ A_1 \exp(\gamma_+ z_1) + \gamma_- A_2 \exp(\gamma_- z_1) = \gamma_- a$$

(3.16) is a set of four equations in four unknowns: A_1, A_2, θ, and z_1. If this system can be solved, then we have the exact solution to the traveling wave problem.

Let us now seek a solution to (3.16) in which the upstroke of the pulse is determined by the $A_2 \exp(\gamma_- z)$ term, the downstroke is determined by the $A_1 \exp(\gamma_+ z)$ term, and the plateau is approximately given by $B \exp(-\varepsilon z)$; this is equivalent to requiring the pulse to be shaped like the solution to the ODE described above for $\tau/\tau_h \ll 1$. Accordingly, let us define the new coefficient $C_1 = A_1 \exp(\gamma_+ z_1)$, and assume that C_1 is of order a, i.e., A_1 is of order $\exp(-\gamma_+ z_1)$. Neglecting terms in $\exp(-\gamma_+ z_1)$ and $\exp(\gamma_- z_1)$, (3.16) reduces to:

$$\text{i)} \quad B + A_2 = a$$

$$-\varepsilon B + \gamma_- A_2 = \gamma_+ a$$

$$\text{ii)} \quad B \exp(-\varepsilon z_1) + C_1 = a$$

$$-\varepsilon B \exp(-\varepsilon z_1) + \gamma_+ C_1 = \gamma_- a$$

In this approximation, the speed may be determined by the behavior of (3.17) i) alone, and the pulse length z_1 is then determined from the speed derived from i), along with the solution of ii). Thus the speed is determined solely by the behavior of the leading edge of the wave. This is a realistic result; wavelengths associated with the pulse as a whole must be of the order of tens of centimeters, since the pulse duration is ≈ 300 milliseconds and the propagation speed is ≈ 2 meters/ second. These long wavelengths are of the same length scale as the whole fiber, so the front of the wave is the only part that can be said to propagate in any meaningful sense. This uncoupling of the leading from the trailing edge is exactly the behavior we want from a model of Purkinje fiber action potential.

In the zeroth order approximation in ϵ, we find the speed of the wave to be exactly that of the traveling front of a change of state waveform for a pure threshold process without recovery (Peskin [18], pp. 261-3). The zeroth order approximation θ_o to the speed θ is:

$$\theta_o^2 = \frac{(\rho - 2)^2}{\rho - 1}$$

where $\rho = \dfrac{E_o}{a}$.

We now turn to the outer expansion, i.e. time scales on the order of τ_h. With the new independent variables $s = t/\tau_h$ and $y = x/\lambda$ (3.10) becomes:

$$u_{yy} = -\frac{\tau}{\tau_h} u_s - E_p H(u-a)h + u$$

$$h_s = 1 - H(u-a) - h$$

As above, we look for traveling waves. Write $z = \dfrac{y}{\phi} + s$, $u(y,s) = U(z)$, and $h(y,s) = h(z)$. U and H must satisfy:

$$\frac{1}{\phi^2}U'' = \epsilon U' + U - E_o H(u-a)h$$

$$h' = 1 - H(U-a) - h \qquad\qquad (3.18)$$

By dimensional analysis, we see that $\phi = \dfrac{\theta}{\epsilon}$.

As before, we require pulse shaped solutions, i.e. $U(z) \geqslant a$ iff $0 \leqslant z \leqslant z_1$, so in $(0, z_1)$ $h = e^{-s}$, and therefore in $(0, z_1)$ (3.18) becomes:

$$\frac{\varepsilon^2}{\theta^2} U'' = \varepsilon U' - E_o e^{-z} + U.$$

To zeroth order in ε, $U = E_o e^{-z}$ and we may approximate z_1 by:

$$a = E_o e^{-z_1}$$

The zeroth order approximation to (3.18) for $z < 0$ or $z > z_1$ is $U = 0$. This can be matched to the above approximation $U = E_o e^{-z}$ at $z = 0$ and $z = z_1$ by patching the two regions with expansions in the fast time scale. In the slow time scale, the solution rises from a to E_o at $z = 0$ and decays from a to 0 at $z = z_1$ exponentially with time constant of the order of ε, since the characteristic roots of (3.18) with $U \leq a$ are $\frac{\gamma_{\pm}}{\varepsilon}$ where $\gamma_{\pm}$ are the same as in equation 3.15. The form of the solution in this long time scale is shown in figure 21.

This model is a very crude one, and in fitting its behavior to experiment, some compromises must be made. To see this, let us refer back to (3.10):

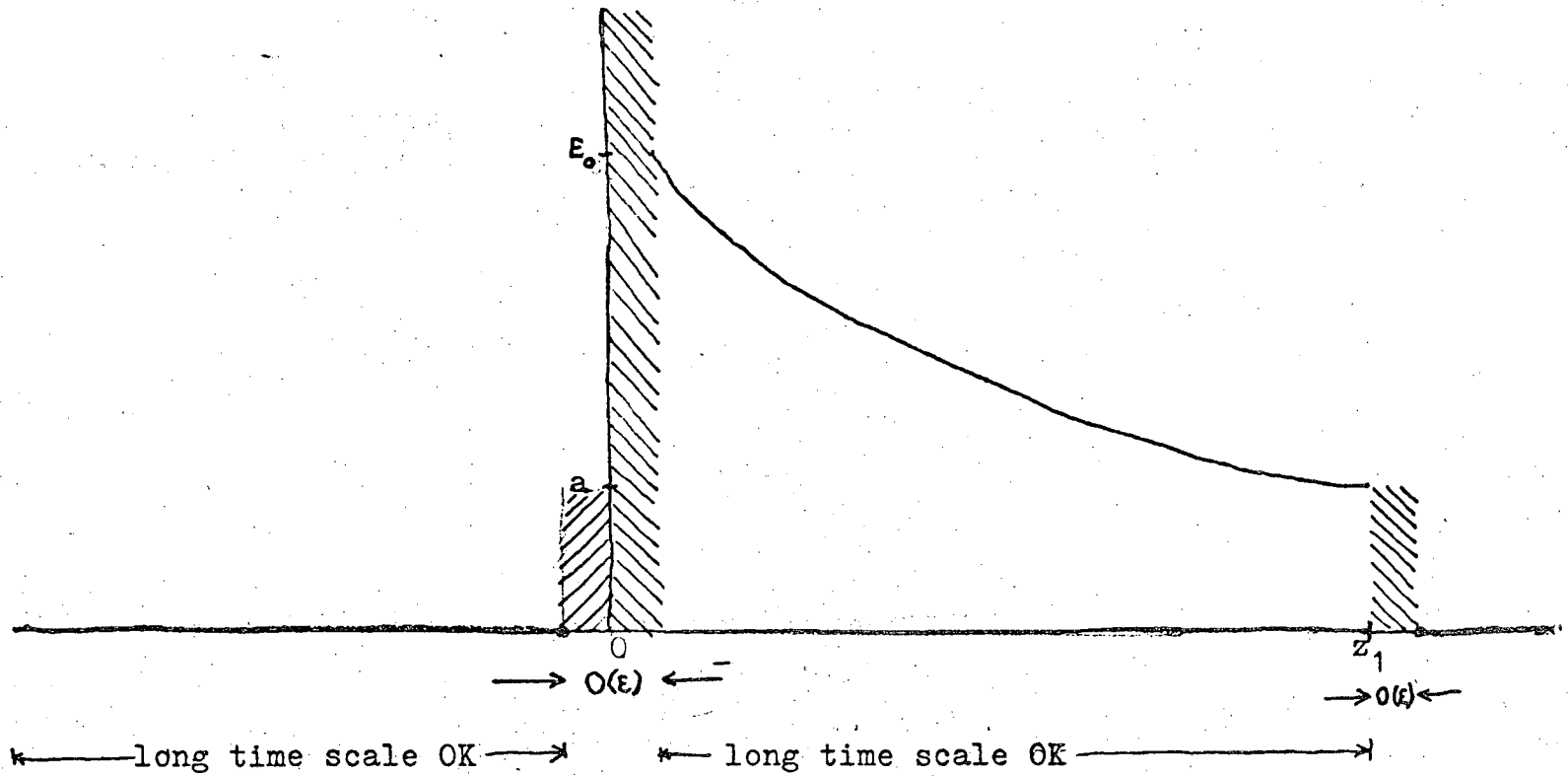$$\frac{\lambda^2}{\tau} u_{xx} = u_t + \frac{1}{\tau} u - \frac{E_o}{\tau} H(u-a)h$$

$$h_t = \frac{1 - H(u-a) - h}{\tau_h}$$

Now transform to the moving coordinate $\zeta = \frac{x}{c} + t$, and look for traveling wave solutions of the form $u(x,t) = U(\zeta)$.

We then have:

Figure 21

The Long Time Approximation
Form of Solution and Region of Validity

hatched areas are regions of validity
for the short time approximation

$$\frac{\lambda^2}{c^2\tau}U'' = U' + \frac{1}{\tau}U - \frac{E_o}{\tau}H(U-a)h$$

$$h' = \frac{1-H(U-a)-h}{\tau_h}$$

with boundary conditions as before: $U(\zeta) \to 0$ as $|\zeta| \to \infty$, $U(\zeta_1) = U(0) = a$ for some positive ζ_1. The solution in the region $[0, \zeta_1]$ will look like:

$$U(\zeta) = B\exp(-k\zeta) + A_1\exp(\gamma_+\zeta) + A_2\exp(\gamma_-\zeta)$$

where $k = \frac{1}{\tau_h}$ and $\gamma_\pm = \frac{c^2}{2\lambda^2}\left\{1 + \sqrt{1 + \frac{4\lambda^2}{c^2\tau^2}}\right\}$

Assume $\frac{\lambda^2}{c^2} \ll \tau^2$ this is the assumption that the propagation of the front is the fastest process in the problem.

Then: $\sqrt{1 + \frac{4\lambda^2}{c^2\tau^2}} \approx 1 + \frac{2\lambda^2}{c^2\tau^2}$

and $\gamma_- \approx \frac{-1}{\tau}$. We assume as before that the $A_1\exp(\gamma_+\zeta)$ term remains unimportant near the leading edge. The boundary conditions then become:

$$A_2 + B = a$$

$$\gamma_-A_2 - kB = \gamma_+a$$

Since $k \ll |\gamma_-|$, $U' \approx \gamma_-A_2$ near the threshold crossing at $\zeta = 0$. We also have: $A_2 = a-B$ and $B \approx E_o$, so $U'(0) \approx \frac{-a-E_o}{\tau}$.

But the peak amplitude will be of the same order as B (recall that the shape of the plateau is approximately $Be^{-k\zeta}$). Thus, if we pick $\tau \approx 10$ milliseconds in accordance with observation (3) and ask for the peak time

derivative of the potential to be around 1000 V/sec as is observed ex-
perimentally, we find amplitudes in the neighborhood of 10 volts!

In the actual numerical simulations, we have chosen to compromise the
rising speed of the pulse rather than tolerate such unrealistically high
peak amplitudes. Parameters used in the numerical simulations described
in chapters four and five were chosen as follows:

$$E_o = 225\text{mV}$$

$$a = 30\text{mV}$$

$$\tau = 5\text{ms}$$

$$\tau_h = 100\text{ms}$$

$$\lambda = 2\text{mm}$$

Numerical solution of 3.17 for these values yields speeds near 1m/sec, and
a pulse duration of approximately 200ms. The amplitude is somewhat high at
approximately 180mV, and the total rise time is rather slow at 16ms, but
still fast on the time scale of the relevant experiments which lasted
several seconds.

It is assumed that the nonlinear characteristics of the membrane are
due to action of some structures (i.e. pores or carriers) at specific sites
at the membrane. Each site is assumed to have kinetics described by:

$$i_{\substack{\text{individual} \\ \text{site}}} = H(u-a)h; \quad \frac{dh}{dt} = \frac{1 - H(u-a) - h}{\tau_h}$$

and the parameter E_o in the foregoing sections is proportional to the
density of active sites on the membrane. Thus if we assume that the action

of some blocking agent is to clog up the individual sites, we may model the blocked fiber by:

$$\frac{\lambda^2}{\tau} u_{xx} = u_t + \frac{1}{\tau} u - B(x) \frac{E_o}{\tau} H(u-a)h$$

$$(3.19)$$

$$h_t = \frac{1 - H(u-a) - h}{\tau_h}$$

where $B(x)$ is the proportion of unblocked active sites.

The action of poisons that interfere with the excitation process by changing the kinetics of each individual site could be modeled by multiplying a or τ_h by a suitable function of x or t.

For various choices of $B(x)$, delay, block and one-way conduction can be observed in the numerical solution of (3.19). The numerical techniques used to solve (3.19) will be discussed in Chapter IV, and the results will be exhibited in Chapter V.

3. <u>The Pathological Case:</u> $\frac{\tau}{\tau_h} \gg 1$

Although solutions of the space-clamped system in this case look much like those of the space clamped system for $\frac{\tau}{\tau_h} \ll 1$, the two traveling wave cases are very different. In fact, the only traveling waves that exist in the limiting case $\frac{\tau_h}{\tau} = 0$ (as noted above, this corresponds to a nonlinear element that injects a finite charge across the membrane instantaneously when a given threshold potential is reached). are moving cusps, where the peak is at $x \pm \theta t = 0$, for some θ.

We shall now derive the differential equation for traveling waves in this case. As noted in Section 1, we must modify the current-voltage

relation so that the charge injected by the nonlinear conductor remains constant independent of τ_h; we will then derive the equation for the traveling wave case exactly as before, by scaling x and t appropriately and then making a transformation to a moving frame of reference.

As before, we choose the length constant λ as our scale length; therefore we define the new variable $y = x/\lambda$. The time will be scaled to the passive time constant τ, which, in this case is the slowest time constant in the problem. Now write $\tau/\tau_h = 1/\varepsilon$. The modification to (3.3) that yields the constant charge property we wish to incorporate in the model currently under discussion can be made by writing E_o/ε instead of E_o in (3.10). Our new time variable is $s = t/\tau$ as described above, and we shall write the solution variable in the new cooordinates as: $u(x,t) = v(y,s)$. Equation (3.10) then becomes:

$$v_{yy} = v_s + \frac{E_o}{\varepsilon} H(v-a)h + v$$

$$h_s = \frac{1 - H(v-a) - h}{\tau_h}$$

Now, in order to get the O.D.E. for traveling waves, we make the transformation $z = y/\theta + s$ and look for solutions of the form $v(y,s) = V(z)$. If such solutions exist, they must satisfy:

$$V'' = \theta^2 V' + \theta^2 V - \frac{\theta^2 E_o}{\varepsilon} H(V-a)h$$

$$h' = \frac{1 - H(V-a) - h}{\varepsilon}$$

(3.20)

Let us now further simplify the model by neglecting the recovery of h and the turning off of $i_{nonlinear}$ after V has decayed to a value less than or equal to a. Equation (3.20) then becomes:

$$V'' = \theta^2 V' + \theta^2 V - \frac{\theta^2 E_o}{\varepsilon} H(z) h$$

$$h = 1, \quad z \leqslant 0; \quad h = \exp(-z/\varepsilon), \quad z \geqslant 0$$

$$V\Big|_{z=0} = a; \quad V'\Big|_{z=0} = \gamma_+ a; \quad |V| \to 0 \quad \text{as} \quad |z| \to \infty$$

where $\gamma_\pm$ are defined as above. For $z \leqslant 0$, $V = \exp(\gamma_+ z)$. For $z \geqslant 0$, (3.21) becomes

$$V'' - \theta^2 V' - \theta^2 V = \frac{-\theta^2 E_o}{\varepsilon} \exp(-z/\varepsilon) \qquad (3.22)$$

First, try a particular solution of the form $B\exp(-z/\varepsilon)$. Substitution into (3.22) yields:

$$\left[\frac{1}{\varepsilon^2} + \frac{\theta^2}{\varepsilon} - \theta^2 \right] B = \frac{-\theta^2 E_o}{\varepsilon}$$

Hence:

$$B = \frac{-\theta^2 E_o}{1/\varepsilon + \theta^2 - \varepsilon\theta^2} = -E_o \frac{\varepsilon\theta^2}{1 + \theta^2\varepsilon - \theta^2\varepsilon^2}$$

Now let us look for solutions of the form

$$V = B\exp(-z/\varepsilon) + A\exp(\gamma_- z)$$

The condition that V be $C^1(\mathfrak{R})$ is then:

$$B + A = a$$

$$\frac{1}{\varepsilon} B + \gamma_- A = \gamma_+ a$$

Upon substitution of the explicit form of B into the above expression, we derive:

$$-E_o \; \frac{\epsilon\theta^2}{1 + \theta^2\epsilon - \theta^2\epsilon^2} + A \;=\; a$$

$$(3.23)$$

$$E_o \; \frac{\theta^2}{1 + \theta^2\epsilon - \theta^2\epsilon^2} + \gamma_- A \;=\; \gamma_+ a$$

A relation for θ may now be derived from the above by eliminating A. This relation is

$$\left[\gamma_- + \frac{1}{\epsilon}\right]\left[\frac{\epsilon\theta^2}{1 + \theta^2\epsilon - \theta^2\epsilon^2}\right] \;=\; (\gamma_+ - \gamma_-)\,\frac{a}{E_o}$$

In the case $\epsilon = 0$, we find $B = 0$, $A = a$, and

$$\frac{E_o}{a}\,\theta^2 + \gamma_- \;=\; \gamma_+$$

Hence

$$\theta^2 \;=\; (\gamma_+ - \gamma_-)\,\frac{a}{E_o}$$

So,

$$\frac{E_o}{a} \;=\; \sqrt{1 + \frac{4}{\theta^2}}$$

From the above we finally derive

$$\theta^2 \;=\; \frac{4}{E_o^2/a^2 - 1}$$

$$(3.24)$$

This is a degenerate case in which the nonlinear element injects a delta function of current when a given threshold potential is reached. The traveling waves look like moving cusps, unlike the voltage vs. time graph of the space clamped behavior of this system, which rises abruptly to E_o and then decays exponentially with time constant τ, as we saw in

Section 1 of this chapter. From the last equation above, we can see that there will be no traveling waves if $E_o \leqslant a$.

We will now show that the values of θ and A depend smoothly on ε for ε sufficiently small by the rather conventional implicit function theorem argument described on the following pages.

First, for the sake of convenience, divide both equations of (3.23) through by a, and define $q = A/a$ and $r = E_o/a$. Equation (3.23) then becomes

$$-r \left\{ \frac{\varepsilon \theta^2}{1 + \theta^2 \varepsilon - \theta^2 \varepsilon^2} \right\} + q = 1$$

$$r \left[\frac{\theta^2}{1 + \theta^2 \varepsilon - \theta^2 \varepsilon^2} \right] + \gamma_- q = \gamma_+$$

Now write

$$f_1(\theta, g; \varepsilon) = (g - 1)(1 + \theta^2 \varepsilon - \theta^2 \varepsilon^2) - r\varepsilon \theta^2$$

$$f_2(\theta, g; \varepsilon) = r\theta^2 + (\gamma_- g - \gamma_+)(1 + \theta^2 \varepsilon - \theta^2 \varepsilon^2)$$

Taking partials evaluated at $\theta = \theta_o = 2/(r^2 - 1)^{\frac{1}{2}}$, $q = 1$, $\varepsilon = 0$, we find

$$\frac{\partial f_1}{\partial g} = 1; \qquad \frac{\partial f_1}{\partial \theta} = 0$$

$$\frac{\partial f_2}{\partial g} = \gamma_- ; \qquad \frac{\partial f_2}{\partial \theta} = 2r\theta + \frac{\partial}{\partial \theta}(\gamma_- - \gamma_+)$$

We have, from the definitions of $\gamma_\pm$ that

$$\gamma_+ - \gamma_- = (\theta^4 + 4\theta^2)^{\frac{1}{2}}$$

and hence

$$\frac{\partial}{\partial \theta}\,(\gamma_+ - \gamma_-) = \frac{\partial}{\partial \theta}\,\sqrt{\theta^4 + 4\theta^2} = \frac{4\theta^3 + 8\theta}{2\sqrt{\theta^4 + 4\theta^2}} = \frac{2\,{}^2 + 4}{\sqrt{\theta^2 + 4}}$$

Recall from (3.24) that $\theta_o^2 = 4/(r^2 - 1)$, so

$$\frac{\partial}{\partial \theta}\,(\gamma_+ - \gamma_-) = \left(\frac{8}{r^2 - 1} + 4\right) \Big/ \left(\frac{4}{r^2 - 1} + 4\right)^{\frac{1}{2}}$$

$$= \left(\frac{4}{r^2 - 1} + 2\right) \Big/ \left(\frac{1}{r^2 - 1} + 1\right)^{\frac{1}{2}}$$

$$= \frac{\sqrt{r^2 - 1}}{r}\,\frac{2(r^2 + 1)}{r^2 - 1} = 2(r^2 + 1)\,/\,[\,r(r^2 + 1)\,]$$

and thus

$$\frac{\partial f_2}{\partial \theta}\Bigg|_{\theta = \theta_o} = \frac{4r}{\sqrt{r^2 - 1}} - \frac{2(r^2 + 1)}{r\sqrt{r^2 - 1}} = \frac{2\sqrt{r^2 - 1}}{r}$$

Hence

$$\begin{pmatrix} \dfrac{\partial f_1}{\partial g} & \dfrac{\partial f_1}{\partial \theta} \\[2ex] \dfrac{\partial f_2}{\partial g} & \dfrac{\partial f_2}{\partial \theta} \end{pmatrix} = \begin{pmatrix} 1 & 0 \\[2ex] \gamma_- & \dfrac{2\sqrt{r^2 - 1}}{r} \end{pmatrix}$$

is nonsingular unless $r = 1$, a case which we have excluded from consideration, so for all $r > 1$, q and θ may be expressed as smooth functions of ε in some neighborhood of $q = 1$ and $\varepsilon = 0$. The forms of the traveling waves for various values of ε are shown in figure 22. These waveshapes are not strictly comparable, since the speeds vary with the value of ε and thus the scaling of the abscissa is different for each wave; but the decay of the peak amplitude with decreasing ε is readily apparent.

TRAVELING WAVE SHAPES FOR $\tau/\tau_h \gg 1$

FIGURE 22

Wave Amplitude

Displacement in Moving Frame

$\tau/\tau_h = \infty$

$\tau/\tau_h = 100$

$\tau/\tau_h = 50$

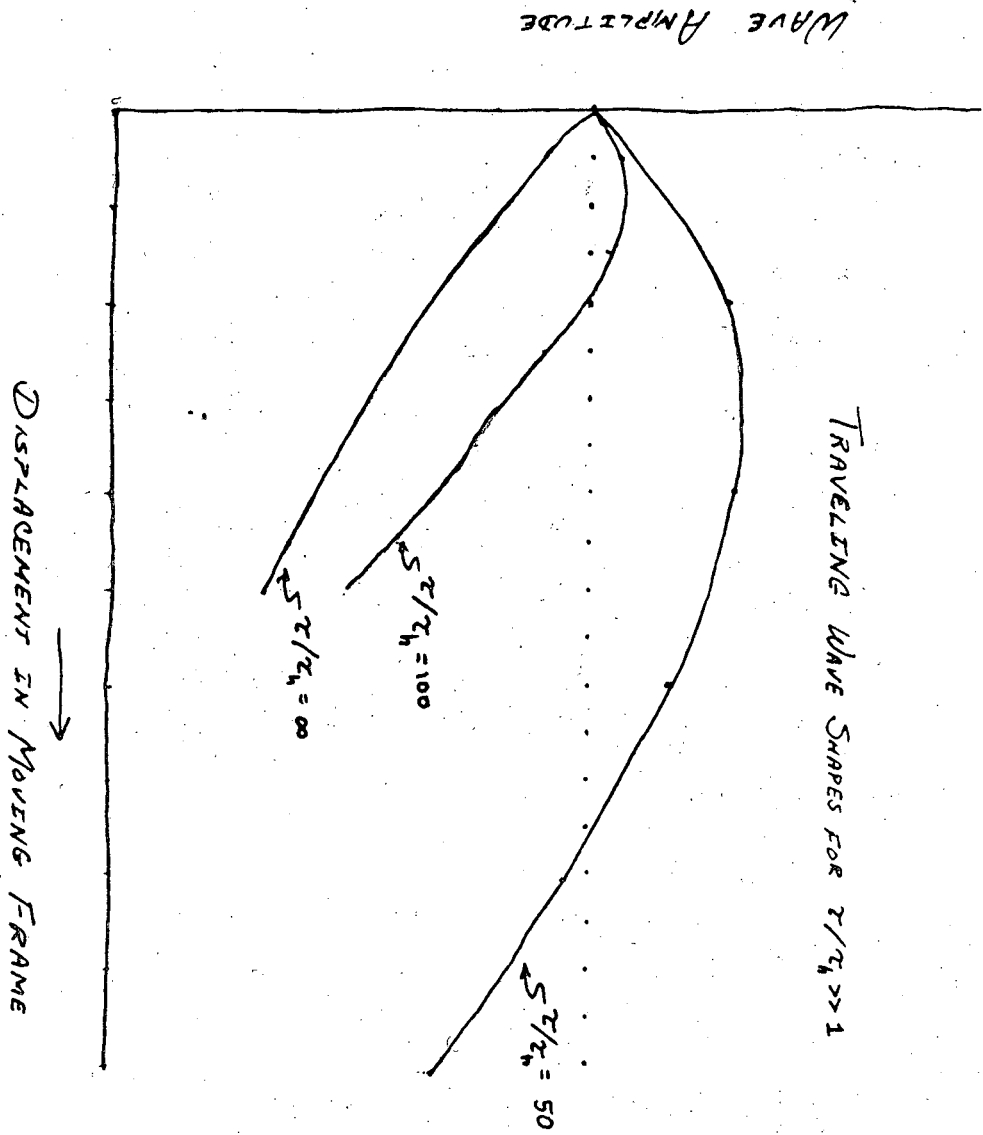## IV. NUMERICAL TECHNIQUES

The model presented above has some obvious conceptual and analytical
advantages: the biophysical intuition for each of the parameters in the
equation is unambiguous, and the traveling wave analysis is easy,
requiring only the solution of some transcendental equations for the
complete solution of the problem for any given combination of parameters.
The case of greatest importance, however, is that of spatial inhomogeneity,
where the traveling wave analysis cannot be used. There is now only one
exact solution known for a model of the form presented above with spatial
inhomogeneities. This solution was presented by John Rinzel (personal
communication), and it will be described in detail below. Perturbation
techniques are also under consideration currently, but the major results
are numerical. The discontinuities in the model present special numerical
problems which must be taken into account in the design of computer
programs for the solution of equations (3.19).

The only solutions we shall consider will be those that are
continuous in time and piecewise analytic in space. Recall that the
longitudinal current is proportional to the space derivative of the
membrane potential, the capacity current is proportional to its time
derivative, and the membrane current is proportional to its second space
derivative. Therefore, the condition that these physical quantities be
finite implies that a solution must have a certain amount of smoothness
in order to have any physiological interest. We shall therefore assume
that sufficiently smooth solutions exist.

It is easy to derive jump conditions for the behavior of the
solution at a threshold crossing. Write the first equation of (3.19) as:

$$\frac{\lambda^2}{\tau} u_{xx} - u_t - \frac{1}{\tau} u = -B(x) \frac{E_o}{\tau} H(u-a)h \qquad (4.1)$$

Now suppose $u = a$ at $x = x_o$. Assume further that $u_x\big|_{x=a} > 0$. Choose $x_+ \geq x_o$ and $x_- \leq x_o$. After evaluating all of the terms of (4.1) at x_+ and x_-, we can form the following difference

$$\left(\frac{\lambda^2}{\tau} u_{xx} - u_t - \frac{1}{\tau} u\right)\bigg|_{x=x_+} - \left(\frac{\tau^2}{\tau} u_{xx} - u_t - \frac{1}{\tau} u\right)\bigg|_{x=x_-} = -B(x_+) \frac{E_o}{\tau} h(x_+,t)$$

If we allow x_- to approach x_+, keeping them on opposite sides of x_o, the $\frac{1}{\tau} u$ terms on the left-hand side cancel because of the continuity of u at x_o, leaving us in the limit with

$$\left[\left(\frac{\lambda^2}{\tau} u_{xx} - u_t\right)\right]\bigg|_{x=x_o} = -B(x_o) \frac{E_o}{\tau} h(x_o,t) \qquad (4.2)$$

where the square brackets denote the size of the jump in the quantity enclosed at the specified point. Note that $B(x)$ need not be continuous, but must have a right and left limit everywhere. In the case of traveling waves, u_t is proportional to u_x, which is proportional to the longitudinal current, which must be continuous in order that the membrane current remain finite, so all of the discontinuity is accounted for by the u_{xx} term. In the space clamped case, $u_{xx} = 0$, and u_t accounts for all of the discontinuity. In the case of a boundary value problem, the values of the jumps in u_t and u_{xx} cannot be readily determined.

With the jump conditions in hand, let us now investigate the effects of using conventional numerical techniques to find approximate solutions to these equations with discontinuities. First, we turn to the space clamp case. We shall limit our discussion to implicit methods in order

to avoid the stability problems that inevitably arise with explicit methods. To simplify matters, we assume that $h \equiv 1$. This should not affect the applicability of our results. We will only consider methods that are known to work when the solution is smooth enough, so the only questions remaining to be settled pertain to the behavior of the scheme in a neighborhood of a threshold crossing. In order to estimate the time course of the upstroke accurately, our method will have to take steps of the same order of magnitude as τ. Since $\tau \ll \tau_h$ in the physiologically interesting case, h will change very little in the course of a few time steps, and can be considered constant. Let I be the total current passing through our space clamped membrane, divided by the membrane capacitance/unit area. The differential equation governing the membrane potential V is

$$\frac{dV}{dt} = \frac{-1}{\tau}V + \frac{E_o}{\tau}H(V-a) + I \qquad (4.3)$$

Now let:

    U = the initial potential

    k = the length of the time step

    W = the approximate solution at time $t = k$

    V = the true solution at $t = k$

The backwards difference equation is

$$\frac{W-U}{k} + \frac{1}{\tau}W = I + \frac{E_o}{\tau}H(W-a) \qquad (4.4)$$

Assume $U < a$; the solution to (4.3) is:

$$V = U\exp(-t/\tau) + \tau I(1 - \exp(-t/\tau)) \ ,$$

and this remains valid up to a threshold crossing.

Now let us attempt to solve (4.4) by a method of successive approximations. Rewrite (4.4) as

$$W = \frac{U + kI}{1 + (k/\tau)} + \frac{kE_oH(W - a)}{\tau(1 + (k/\tau))} \equiv F(W) \tag{4.5}$$

The method of successive approximations will predict a threshold crossing if:

$$\frac{U + kI}{1 + (k/\tau)} \geq a$$

This is a sufficient condition; it is also necessary if U is used as the initial guess. Its necessity has not been checked in other cases. This can be illustrated by figure 23.

Let us now check the conditions under which the true solution will cross threshold. Expanding the true solution at $t = k$ in powers of $\frac{k}{\tau}$ yields

$$V = U\left(1 - (\frac{k}{\tau}) + \frac{1}{2}(\frac{k}{\tau})^2 - \frac{1}{6}(\frac{k}{\tau})^3 + \ldots\right) + \tau I\left((\frac{k}{\tau}) - \frac{1}{2}(\frac{k}{\tau})^2 + \frac{1}{6}(\frac{k}{\tau})^3 - \ldots\right)$$

$$= U + kI - (\frac{k}{\tau})(U + \frac{1}{2}kI) + 0(\frac{k^2}{\tau^2}) \tag{4.6}$$

If the method of successive approximations predicts a threshold crossing, then (4.5a) is satisfied and

$$V \geq a(1 + \frac{k}{\tau}) - U\frac{k}{\tau} + \frac{1}{2}U\frac{k^2}{\tau^2} - \frac{1}{2}\tau I(\frac{k}{\tau})^2 + 0(\frac{k^3}{\tau^3})$$

$$= a + (a - U)\frac{k}{\tau} + \frac{1}{2}U(\frac{k}{\tau})^2 - \frac{1}{2}\tau I(\frac{k}{\tau})^2 + 0(\frac{k^3}{\tau^3})$$

$$\geq a + \frac{1}{2}(U - \tau I)(\frac{k}{\tau})^2 + 0(\frac{k^3}{\tau^3})$$

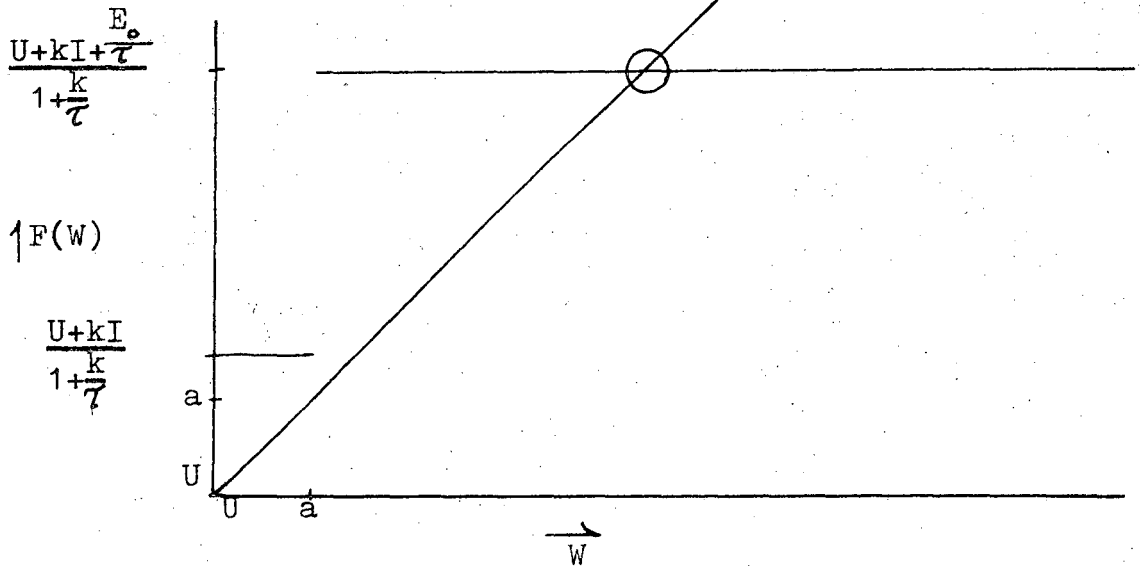since we have assumed $a \geq U$. Therefore, if the method predicts a threshold

Figure 23

The Method of Successive Approximations

i) Threshold Crossing Not Predicted
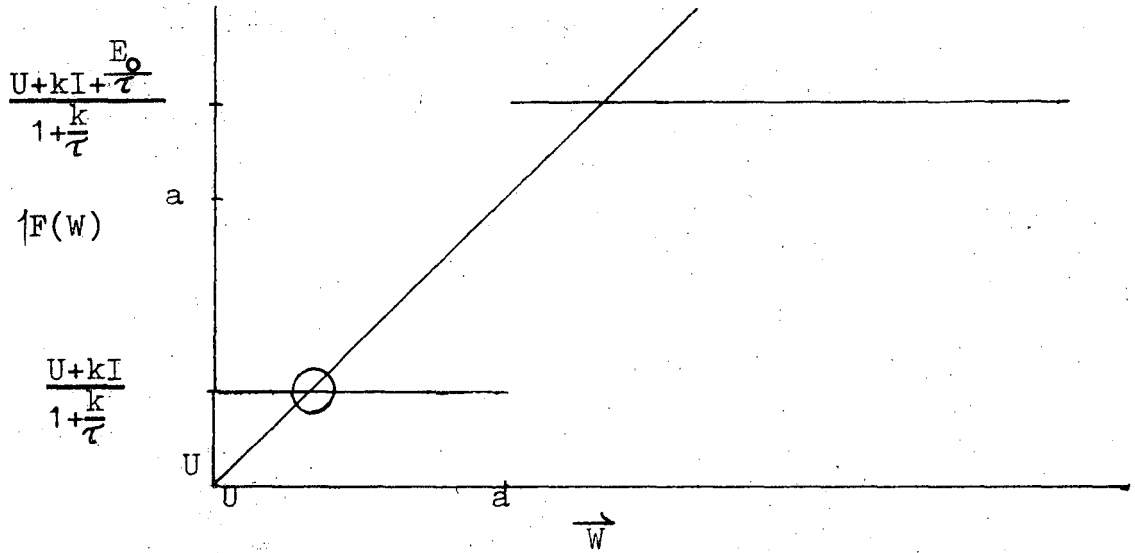
ii) Threshold Crossing Predicted

crossing, within a given time step then there will be one, up to an

error of the same order as the accuracy of the method itself.

Since we are now assured that the method will predict no spurious

threshold crossings, let us attempt to estimate the errors introduced

when the threshold is crossed. The condition that a threshold crossing

be predicted is: $U + kI/1 + (k/\tau) > a$. Let us suppose that this is the

case. Then

$$W = \frac{U + kI + k(E_o/\tau)}{1 + (k/\tau)}$$

Now suppose the true solution crosses threshold at $t = t_o \leqslant k$. Then the

true solution V at $t = k$ is given by

$$V = U\exp(-k/\tau) + I(1 - \exp(-k/\tau)) + E_o(1 - \exp[(k - t_o)/\tau])$$

Expanding V and W in powers of $k/$ and subtracting yields

$$V - W = E_o \frac{(k - t_o)}{\tau} + 0(k^2)$$

Thus, in a time step in which a threshold crossing occurs, the

discontinuity introduces an error proportional to the fraction of the

step in which the system remained below threshold. This is due to the

fact that in such a step, the approximate solution is computed as if the

system had been above threshold for the entire step. The error checking

code should therefore maneuver the step size in time in order to come

close to having the approximate solution actually take on the threshold

value. This is the behavior observed in practice.

The problem of dealing with the discontinuity becomes more difficult

for the partial differential equation with inhomogeneities in space,

since we may no longer deal with traveling waves. We shall see below

that conventional methods will introduce large errors in the case of a discontinuity in u_{xx}.

With appropriate scaling, the model may be written as

$$u_t + u - u_{xx} = H(u-a)h$$

<div align="right">(4.7)</div>

$$h_t = \frac{1-H(u-a)-h}{\tau_h}$$

We are interested in the initial-boundary value problem for (4.7) on $[0,1]$ subject to

$$u_x(0,t) = u_x(1,t) = 0$$

$$u(x,0) = f(x)$$

·We have chosen the so-called sealed and boundary condition, i.e., the condition that there is no current flow out of the fiber at the ends.

We shall first illustrate the difficulty that arises if the discontinuity is ignored, and u_{xx} is evaluated by second differences on a fixed grid. Assume u is $C^1([0,1])$ and piecewise analytic; assume further, to illustrate the problem, that u is decreasing on $(jk,(j+1)k)$ and that $u = a$ at $x = jk+k'$, as in figure 24, where k is the distance between adjacent grid points. Let u_n be defined as $u(nk)$. Since u is piecewise analytic in space, we have

$$u_{j-1} = u_j - ku_{jx} + \frac{k^2}{2} u_{jxx} - \frac{k^3}{6} u_{jxxx} + \ldots$$

$$a = u_j + k'u_{jx} + \frac{k'^2}{2} u_{jxx} + \frac{k'^3}{6} u_{jxxx}$$

Let

$$u_x = \left.\frac{\partial u}{\partial x}\right|_{xjk+k'} ; \quad u_{xx}^+ = \left.\frac{\partial^2 u}{\partial x^2}\right|_{u \to a^+} ; \quad u_{xx}^- = \left.\frac{\partial^2 u}{\partial x^2}\right|_{u \to a^-}$$

Figure 24

Assumed Graph of u versus x in an Interval

Containing a Threshold Crossing
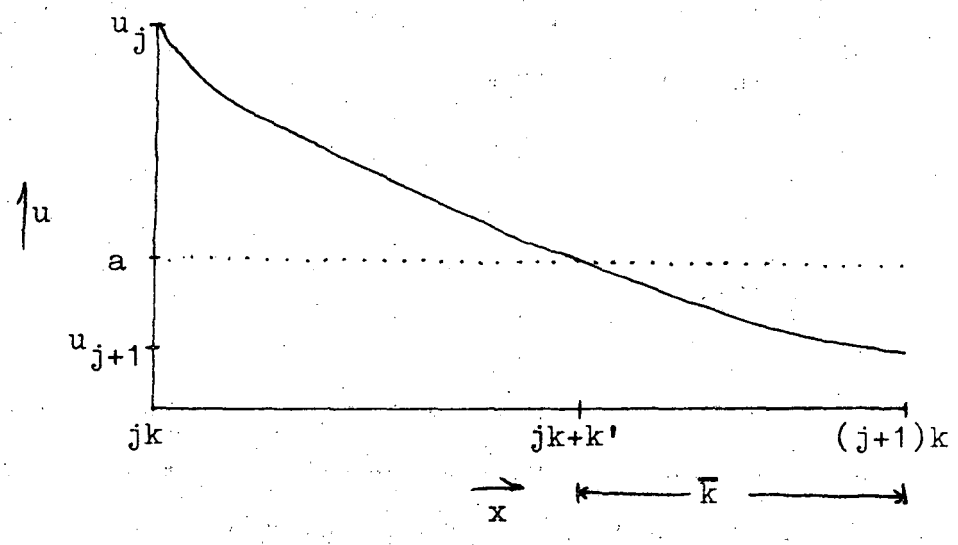
Expanding u in Taylor series about the threshold crossing, and then re-expanding in terms of u_j, we find

$$u_{j+1} = a + ku_x + \frac{k}{2} u_{xx}^- + \frac{k}{6} u_{xxx}^- + \dots$$

$$= u_j + k'u_{jx} + \frac{k'^2}{2} u_{jxx} + \frac{k'^3}{6} u_{jxxx}$$

$$+ \bar{k}(u_{jx} + k'u_{jxx} + \frac{k'^2}{2} u_{jxxx} + \dots)$$

$$+ \frac{\bar{k}^2}{2} (u_{jxx} + k'u_{jxxx} + \frac{k'^2}{2} u_{jxxx} - u_{xx}\Big|_-^+)$$

$$= u_j + ku_j + \frac{k^2}{2} u_{jxx} - \frac{\bar{k}^2}{2} u_{xx}\Big|_-^+ + \dots$$

where

$$u_{xx}\Big|_-^+ = \text{the jump in } u_{xx} \text{ from } a^- \text{ to } a^+$$

Hence

$$\frac{u_{j+1} - 2u_j + u_{j-1}}{k^2} = u_{jxx} - \frac{\bar{k}^2}{2k^2} u_{xx}\Big|_-^+ + \dots$$

A sequence of grids can clearly be chosen with the property that k goes to 0 and $\bar{k}/k$ goes to 1. So, with the usual second difference formula, the discontinuity introduces an error which may be 0(1) as k goes to 0.

Suppose we interpolate to find the point where u crosses threshold. If the interpolation error in the location of the threshold crossing is e, the distance of the interpolated point from the left end of the interval is k*, and the value of u at jk + k* is u*, then calculations identical to those above yield:

$$\frac{u_{j-1} - u_j}{k(k + k^*)} + \frac{u^* - u_j}{k^*(k + k^*)} = \frac{1}{2} u_{jxx} + \frac{e^2}{4k^*(k + k^*)} u_{xx} \Big|_-^+ + \cdots$$

which is acceptable since $e = o(k)$ for any respectable interpolation scheme; but since we do not know u^*, the formula we must use is

$$\frac{u_{j-1} - u_j}{k(k + k^*)} + \frac{a - u_j}{k^*(k + k^*)} = \frac{u_{j-1} - u_j}{k(k + k^*)} + \frac{u^* - u_j}{k^*(k + k^*)} + \frac{a - u^*}{k^*(k + k^*)}$$

In the case of linear or parabolic interpolation, this rightmost term can be $0(1)$ as k goes to 0. A method that has been found to work is the construction of a weighted average of two parabolic interpolates, one from each side of the interval in which the threshold crossing takes place, with the weights chosen in such a way that $\frac{a - u^*}{k^*(k + k^*)}$ goes to 0 like e/k as k goes to 0.

The interpolating parabola through u_{j-1}, u_j and u_{j+1} is given by

$$P_j(x) = \frac{1}{2} \frac{u_{j+1} - 2u_j + u_{j-1}}{k^2} x^2 + \frac{1}{2} \frac{u_{j+1} - u_{j-1}}{k} + u_j \qquad (4.10)$$

Define h_+^* such that $0 \leqslant h_+^* \leqslant k$ and $P_j(h_+^*) = a$. Now put $\bar{k}_- = k - h_-^*$, where $jk + h_-^*$ is the point where the parabola passing through u_j, u_{j+1}, and u_{j+2} takes on the value a in the interval between $x = jk$ and $x = (j+1)k$. $\bar{k}_-$ satisfies

$$\frac{1}{2} \frac{u_{j+2} - 2u_{j+1} + u_j}{k^2} \bar{k}_-^2 - \frac{u_{j+2} - u_j}{2k} \bar{k}_- + u_{j+1} = a \qquad (4.11)$$

Expanding (4.10) and (4.11) in Taylor series about jk and $(j+1)k$ respectively yields

$$a = u_j + h^* + u_{jx} + \frac{h^{*2}}{2} u_{jxx} - \frac{h^*_+}{4h} \bar{k}^2 u_{xx}\Big|^+_- - \frac{h^{*2}_+}{2h^2} \bar{k}^2 u_{xx}\Big|^+_- + O(k^2)$$

$$\text{(4.12)}$$

$$a = u_{j+1} - \bar{k} u_{j+1_x} + \frac{\bar{h}^2_-}{2} u_{j+1_{xx}} + \frac{\bar{h}_- k'^2}{4k} u_{xx}\Big|^+_- + \frac{\bar{h}_- k'^2}{2h^2} u_{xx}\Big|^+_- + O(h^3)$$

$$\text{(4.13)}$$

We have also

$$u^*_+ = u_j + h^* + u_{jx} + \frac{h^{*2}_+}{2} u_{jxx} + O(k^2) \qquad \text{(4.13a)}$$

$$u^*_- = u_{j+1} - \bar{k}_- u_{j+1_x} + \frac{\bar{k}^2_-}{2} u_{j+1_{xx}} + O(k^2) \qquad \text{(4.13b)}$$

Let us now put $k^* = \alpha h^*_+ + \beta h^*_-$, where $\alpha + \beta = 1$. Since

$$a = u_j + k' u_{jx} + \frac{k'^2}{2} u_{jxx} + O(h^2) \qquad \text{(4.14)}$$

we derive

$$0 = -k_+ u_{jx} + u_{jxx} \frac{h^{*2}_+}{2} - \frac{k'^2}{2} + O(h^2)$$

by subtracting (4.14) from (4.12), where $k_+ \equiv h^*_+ - k'$ and thus we are reassured that $k_+ = O(k^2)$ in any domain bounded away from the boundary and from relative extrema; hence we may approximate u^* by its linear interpolate $\alpha u^*_+ + \beta u^*_-$, and in so doing, introduce an error which is $O(e) = O(k^2)$, which will not contribute an $O(1)$ term to our estimate for u_{jxx}.

So, multiplying (4.12) and (4.13a) by (4.13) and (4.13b) and β,

and forming $-\alpha(4.13a) - \beta(4.13b)$, we find

$$a - u^* + 0(h^2) = \frac{-\alpha}{2} \bar{k}^2 u_{xx} \Big|_-^+ \left(\frac{h_+^*}{2k} + \frac{h_+^{*2}}{k^2} \right)$$

$$+ \frac{\beta}{2} k'^2 u_{xx} \Big|_-^+ \left(\frac{\bar{h}_-}{2k} + \frac{\bar{h}_-^2}{k^2} \right) + 0(k^2) \qquad (4.15)$$

Thus if we choose

$$D = h_+^{*2} \left(\frac{\bar{h}_-}{2k} + \frac{\bar{h}_-^2}{k^2} \right) + \bar{h}_-^2 \left(\frac{h_+^*}{2k} + \frac{h_+^{*2}}{k^2} \right)$$

$$\alpha = \frac{1}{D} \left[h_+^{*2} \left(\frac{\bar{h}_-}{2k} + \frac{\bar{h}_-^2}{k^2} \right) \right]$$

$$(4.16)$$

$$\beta = \frac{1}{D} \left[\bar{h}_-^2 \left(\frac{h_+^*}{2k} + \frac{h_+^{*2}}{k^2} \right) \right]$$

$$h_+^* = k' + k_+ ; \qquad \bar{h}_- = \bar{k} + k_-$$

equation (4.15) becomes

$$a - u^+ + 0(h^2) = \frac{1}{2D} u_{xx} \Big|_-^+ \left[-(k'^2 + 2k'k_+ + k_+^2)\bar{k}^2 \left(\frac{\bar{h}_-}{2k} + \frac{\bar{h}_-^2}{h^2} \right) \left(\frac{h_+^*}{2k} + \frac{h_+^{*2}}{k^2} \right) \right.$$

$$\left. + (\bar{k}^2 + 2\bar{k}k_- + k_-^2)k'^2 \left(\frac{h_+^*}{2k} + \frac{h_+^{*2}}{k^2} \right) \left(\frac{\bar{h}_-}{2k} + \frac{\bar{k}_-^2}{k^2} \right) \right]$$

$$= \frac{1}{2} \left(\frac{h_+^*}{2k} + \frac{h_+^{*2}}{k^2} \right) \left(\frac{\bar{h}_-}{2k} + \frac{\bar{h}_-^2}{k^2} \right) u_{xx} \Big|_-^+ \times$$

$$\times \left(\frac{2\bar{k}k'^2k_- + k_-^2k'^2 - 2k'\bar{k}^2k_+ - k_+\bar{k}^2}{h_+^{*2}\left(\dfrac{\bar{h}_-}{2k} + \dfrac{\bar{h}_-^2}{k^2}\right) + \bar{h}_-^2\left(\dfrac{h_+^*}{2k} + \dfrac{h_+^{*2}}{k^2}\right)} \right)$$

which is at worst $O(kk_+)$ $O(ek)$. Using this method, I have obtained the numerical results described in the next section.

In practice, the partial differential equations under consideration are approximated by the system of ordinary differential equations

$$\underline{u}'(t) = \frac{\lambda^2}{\tau} A(t)\underline{u} + \underline{N}(\underline{u},\underline{h})$$

$$\underline{h}'(t) = \frac{1 - \underline{M}(\underline{u}) - \underline{h}}{\tau_h}$$

(4.17)

where the components of the vectors $\underline{u}$ and $\underline{h}$ are the values of the approximate solutions at selected points x_i in the space interval under consideration, and $\underline{N}$ and $\underline{M}$ are nonlinear vector-valued functions whose components N_j and M_j are given by $B(x_j)\dfrac{E_o}{\tau}H(u_j - a)h$ and $H(u_j - a)$ respectively. $A(t)$ is the matrix of the second difference operator for those points that do not border an interval where a threshold crossing takes place. If a threshold crossing is detected in the interval (x_j, x_{j+1}), the approximate position of the threshold crossing is determined by solving (4.10) and (4.11) for h_+^* and $\bar{k}_-$ respectively, and then forming the weighted average $\alpha h_+^* + \beta\bar{k}_- = k^*$ shown above. For the point x_j, $A(t)$ is the asymmetric second difference operator

$$\frac{1}{2}\left(\frac{u_{j-1} - u_j}{k(k + k^*)} + \frac{a - u_j}{k^*(k + k^*)} \right)$$

where a is expressed as a linear function of u_{j-1}, u_j and u_{j+1} using

the fact that the equation $P_j(h_+^*) = a$ is linear in $\underline{u}$. An analogous

calculation is done for the row of $A(t)$ corresponding to x_{j+1}. The

system (4.17) of O.D.E.'s is solved numerically by Miller's diagonally

implicit second order Runge-Kutta method. The results are presented in

the following chapter.

V.   RESULTS AND CONCLUSIONS

The numerical technique described above yields the results illustrated in figure 25 for a spatially homogeneous fiber 15 millimeters long, sealed at the ends. Note that the amplitude grows as the pulse approaches the distal end of the fiber. This effect is to be expected. One way to view the sealed end boundary conditions is to re-interpret the problem as one in which the solution is symmetric with respect to the sealed end. In this framework, a pulse approaching a sealed end is represented as two pulses converging at the same speed to a point that stays exactly between them. The solution is then a superposition in some sense of the solution and its symmetric image. This effect was observed numerically for Hodgkin-Huxley pulses by Rall and Goldstein (11).

In the case of a spatially inhomogeneous fiber, very little can be said analytically. In the case of an infinite fiber stimulated by a point current source at $x = 0$ there is a steady state solution which the fiber probably settles down to after some length of time has elapsed. With appropriate scaling, we may write the equation for this case as

$$u_t + u - u_{xx} = H(u-a)h + U\delta(x)$$

$$h_t = \frac{1 - H(u-a) - h}{\tau_h}$$

A steady state solution would be

$$h = \begin{cases} 0, & |x| \leq x_b \\ 1, & |x| > x_b \end{cases} \qquad u = \begin{cases} \tfrac{1}{2}Ue^{-x}, & x \geq 0 \\ \tfrac{1}{2}Ue^{x}, & x < 0 \end{cases} \qquad x_b = \log(\frac{U}{2a})$$

SIMULATION BY SIMPLE MODEL OF THE RESPONSE OF A FIFTEEN MILLIMETER FIBER STIMULATED AT THE LEFT END

FIGURE 25

STIMULUS = 300 MICROAMPS; DURATION = 6.5 MS.
PROXIMAL   3.1 MM FROM LEFT END
MEDIAL   7.6
DISTAL   12.1
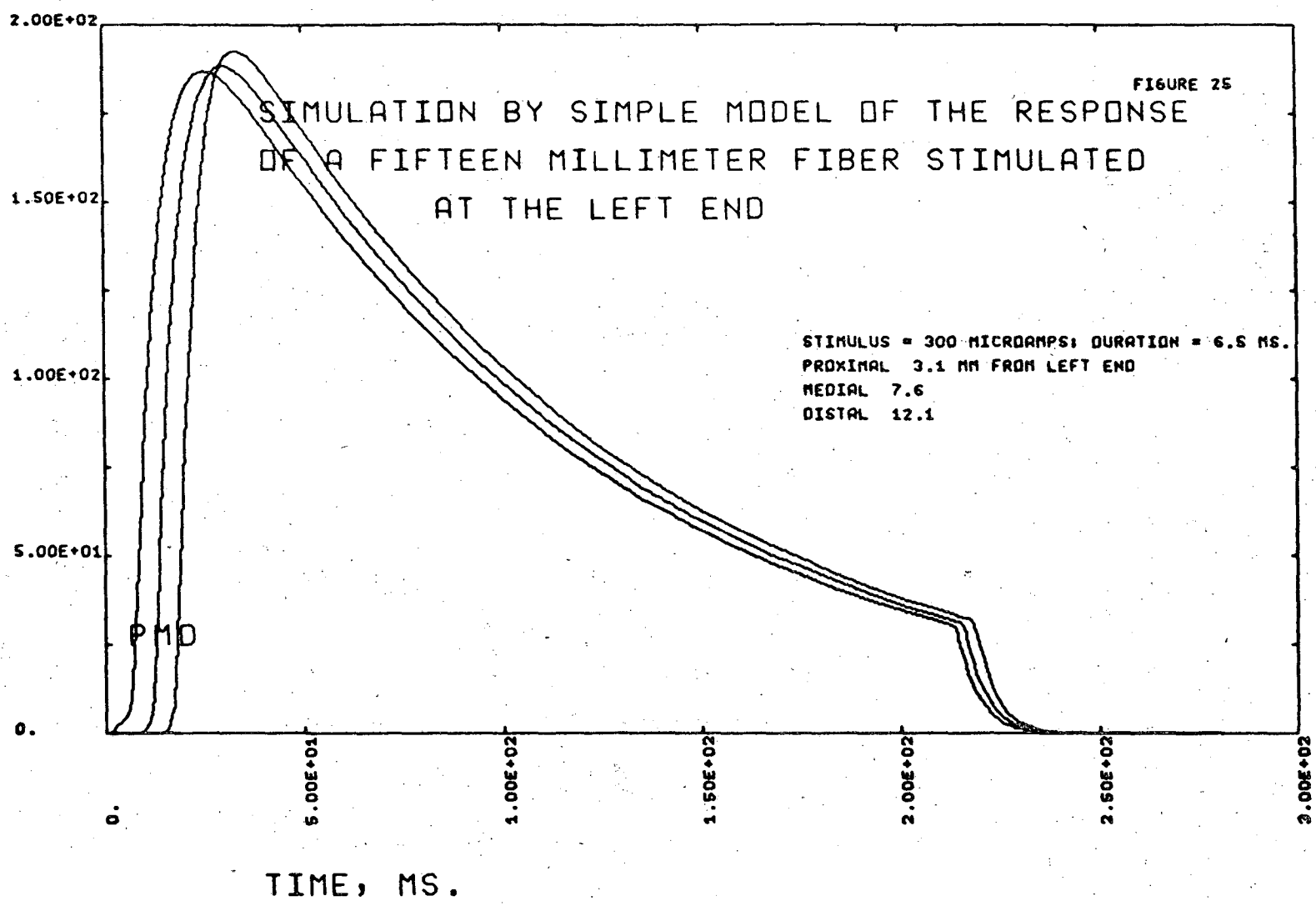
and U is required to be $> 2a$.

The only other exact solution available at this time is for the case $\tau_h = \infty$, for the following conditions

$$u_t \;=\; u_{xx} - u + H(u-a)H(-x)$$

$$u(x,0) \;=\; W(x)$$

where $W(x - \theta t)$ is the traveling wave solution to

$$u_t \;=\; u_{xx} - u + H(u-a)$$

with $u = a$ at $x = \theta t$. This can be solved exactly since it is a linear problem. The solution is

$$u(x,t) \;=\; \int_{-\infty}^{\infty} K(x-y,t)W(y)\,dy \;+\; \int_{0}^{t}\int_{-\infty}^{0} K(x-y,s)\,ds\,dy$$

where

$$K(x,t) \;=\; \frac{e^{-t}\, e^{-x^2/4t}}{\sqrt{4\pi\tau'}}$$

This solution approaches

$$u(x) \;=\; \begin{cases} 1 - \tfrac{1}{2}e^{x} & x < 0 \\[2mm] \tfrac{1}{2}e^{-x} & x \geqslant 0 \end{cases}$$

for long times. This solution was first proposed by John Rinzel.

Figures 26, 27 and 28 show the numerical results from applying the method described above to equation (3.19) for various choices of the blocking function $B(x)$. Asymmetric forms of $B(x)$ similar to those used in the computation of figures 27 and 28 could have arisen in the preparation
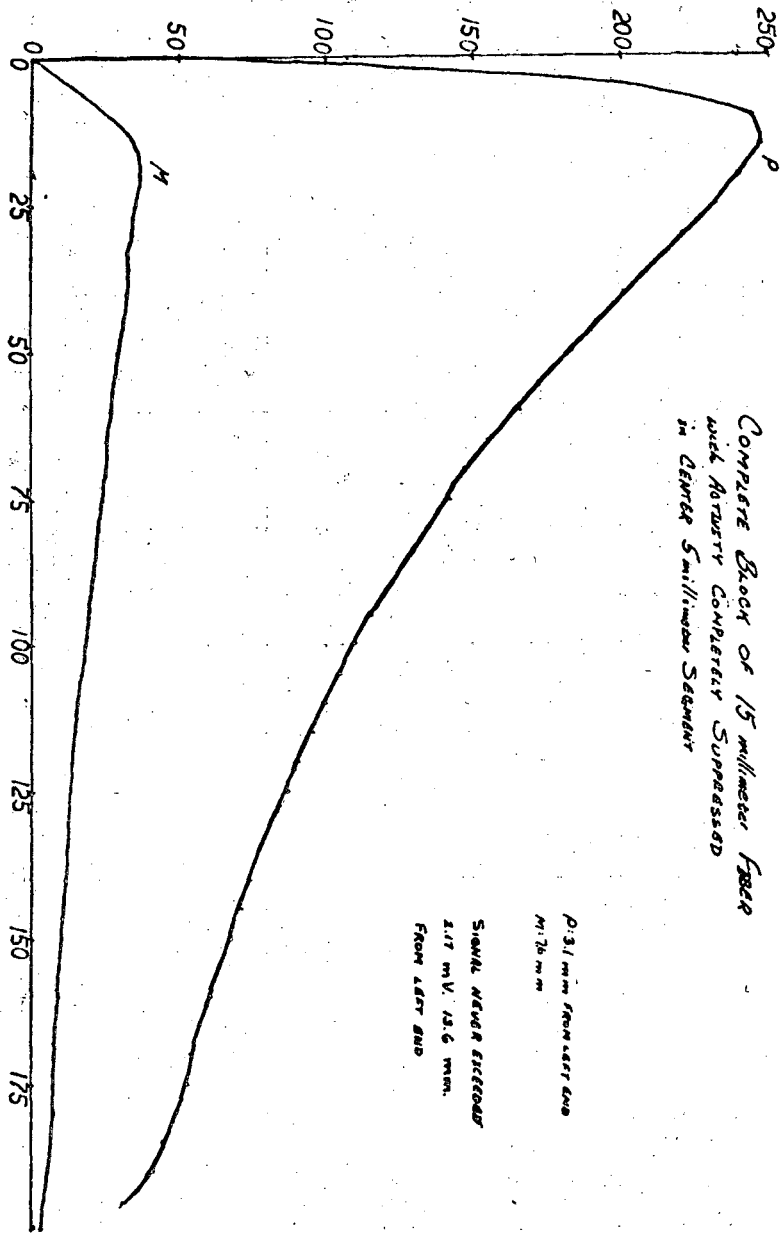
Figure 26

Plot of Potential vs. Time

Complete Block of 15 millimeter Fiber
with Activity Completely Suppressed
in Center 5 millimeter Segment

P: 3.1 mm from left end
M: 7.6 mm

Signal never exceeded
2.17 mV, 13.6 mm.
from left end

CONDUCTION ACROSS ASYMMETRICAL BLOCK

FIBER COMPLETELY BLOCKED 5.1-6.7 mm. FROM LEFT END
BLOCKING FACTOR INCREASES LINEARLY FROM 0 TO 1 6.7-9.7 mm
FROM LEFT END
BLOCKING FACTOR = 1 (i.e. FIBER INTACT) ELSEWHERE

P: 3.1 mm from left end
M: 7.6
D: 12.3

FIGURE 27

Figure 28. BLOCK

MEMBRANE POTENTIAL

TIME, MS

BLOCKING FACTOR DECREASES LINEARLY FROM 3.0-8.0 mm. FROM LEFT END
BLOCKING FACTOR=0, 8.1-9.1 mm. FROM LEFT END
BLOCKING FACTOR=1 ELSEWHERE

P: 3.1 mm. from left
M: 7.6
D: 12.1

used by Cranefield, Hoffman and their coworkers in (2), (4), and (5).
The ager block which was used to depress the excitability of the center
segment of a given fiber had a potassium concentration that was much
higher than the bathing solution. As the bathing solution flowed over
the agar during the experiment, it could have picked up additional
potassium ions and carried them downstream, thus the bathing solution
would have a higher concentration of potassium ions downstream of the block
than upstream. Hence, if we were to travel in the downstream direction
along the outer surface of the fiber we would see the potassium concen-
tration rise sharply as we entered the block and taper off slowly as we
left it.

In figures 26, 27, and 28, delay, block and one-way conduction are
clearly displayed. We may conclude that these effects observed experi-
mentally by Cranefield and Hoffman (4) can be explained in terms of a one
dimensional model, and may not depend on more complicated geometry or the
details of the voltage-current relations of the membrane.

This example of one-way block may actually be a case of asymmetrical
one-for-n block, i.e., the transmission by a depressed segment of one
pulse for every n incident pulses, but the numerical methods developed
above will fail in an attempt to demonstrate one-for-n block, since the
interpolation error for the parabolic interpolate used is proportional to
$1/u_x$, and thus it cannot deal with a relative extremum, which must occur
in the case of one-for-n block. New numerical methods are now being
devised to deal with this problem.

-81-

ACKNOWLEDGMENTS

REFERENCES

(1)   Casten, Cohen and Lagerstrom, "Perturbation Analysis of an Approximation to the Hodgkin-Huxley Theory", Quart. of Appl. Math. 32 (1975) 365-402.

(2)   Cranefield and Hoffman, "Conduction of the Cardiac Impulse", Circ. Res. 28 (1971) 220-233.

(3)   Cranefield and Hoffman, Electrophysiology of the Heart, McGraw-Hill, New York (1960).

(4)   Cranefield, Klein and Hoffman, "Conduction of the Cardiac Impulse", Circ. Res. 28 (1971) 199-219.

(5)   Cranefield, Wit and Hoffman, "Conduction of the Cardiac Impulse", J. Gen. Physiol. 59 (1972) 227-246.

(6)   Dudel, "Excitation Process in Heart Cells", in Electrical Phenomena in the Heart, De Mello, editor; Academic Press, New York (1972).

(7)   FitzHugh, "Mathematical Models of Excitation and Propagation in Nerve", in Biological Engineering, Schwann, editor; McGraw-Hill, New York (1969).

(8)   FitzHugh, "Theoretical Effect of Temperature on Threshold in the Hodgkin-Huxley Nerve Model", J. Gen. Physiol. 49 (1966) 989-1005.

(9)   FitzHugh, "Mathematical Models of Threshold Phenomena in the Nerve Membrane", Bull. Math. Biophys. 17 (1955) 257-278.

(10) Fozzard, "The Membrane Capacitance of Heart Cells", in Electrical Phenomena in the Heart, De Mello, editor; Academic Press, New York (1972).

(11) Goldstein and Rall, "Changes of Action Potential Shape and Velocity for Changing Core Conductor Geometry", Biophys. J. 14 (1974) 731-757.

-83-

(12) Hauswirth, Noble and Tsien, "Mechanism of Oscillatory Activity at
      Low Membrane Potentials in Cardial Purkinje Fibers", J. Physiol.
      200 (1969) 255-265.

(13) Hurewicz, Lectures on Ordinary Differential Equations, second paper-
      back edition, MIT Press, Cambridge, Massachusetts (1970).

(14) Miller, K., Notes on Advanced Numerical Analysis, U.C. Berkeley
      Lecture Notes.

(15) Moore and Ramon, "On Numerical Integration of the Hodgkin and
      Huxley Equations for a Membrane Action Potential", J. Theor. Biol.
      45 (1974) 249-273.

(16) Noble and Tsien, "Outward Membrane Currents Activated in the
      Plateau Range of Potentials in Cardiac Purkinje Fibers", J. Physiol.
      200 (1969) 205-231.

(17) Noble and Tsien, "Reconstruction of the Repolarization Process in
      Cardiac Purkinje Fibers Based on Voltage Clamp Measurements of
      Membrane Current", J. Physiol. 200 (1969) 233-254.

(18) Peskin, Mathematical Aspects of Heart Physiology, Courant Institute
      of Mathematical Sciences, New York (1975).

(19) Rinzel and Keller, "Traveling Wave Solutions of a Nerve Conduction
      Equation", Biophys. J. 13 (1973) 1313-1337.

Reciprocal Time Constant $^{-1}$ vs. Potential
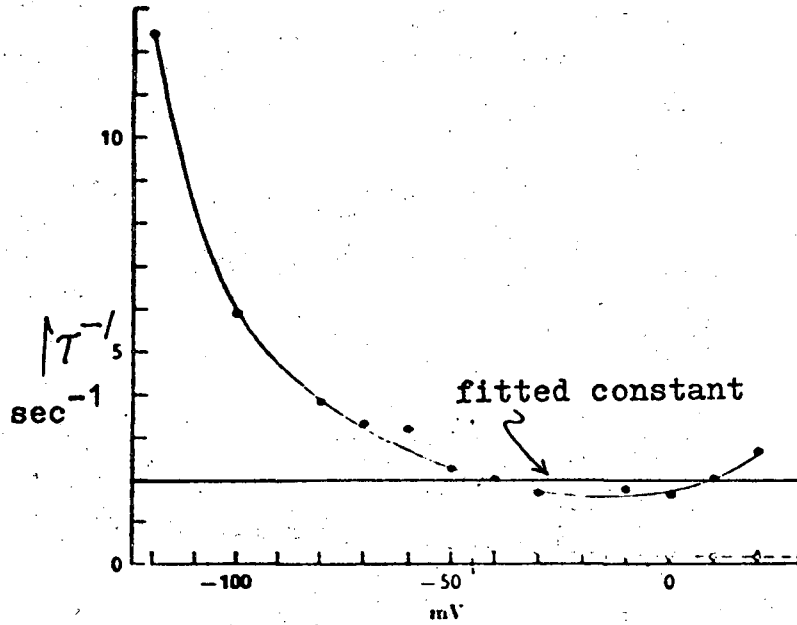
Figure A1

From page 220 of (16)

Steady State Activation of Slow Hyperpolarizing
Current
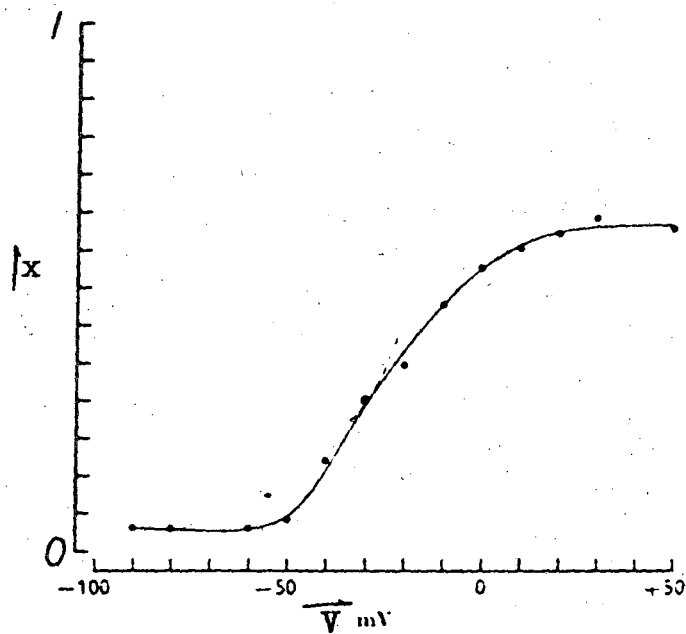
Figure A2

From page 221 of (16)

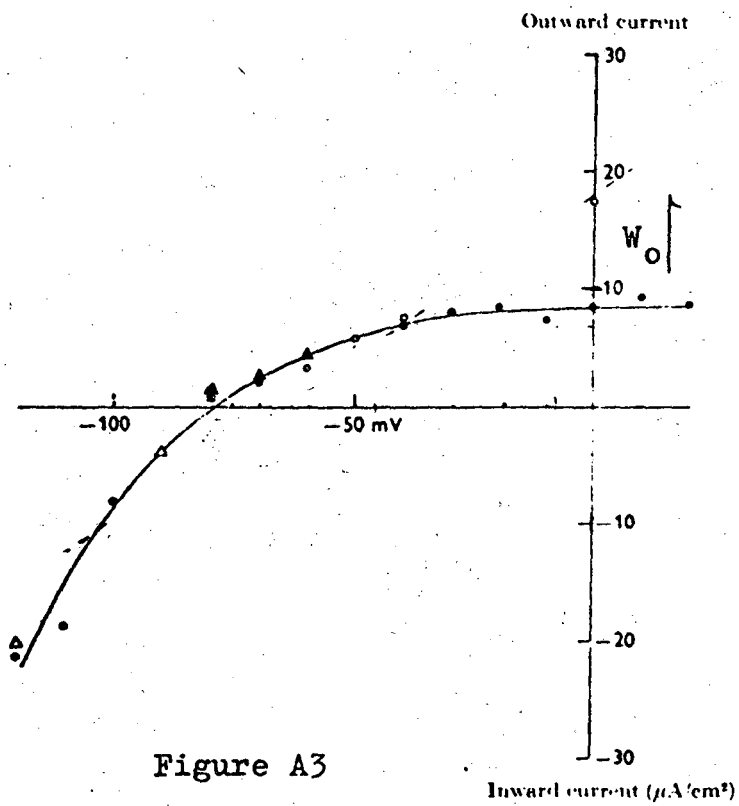Fully Activated Restoring Current vs. Potential

Figure A3

from page 222 of (16)
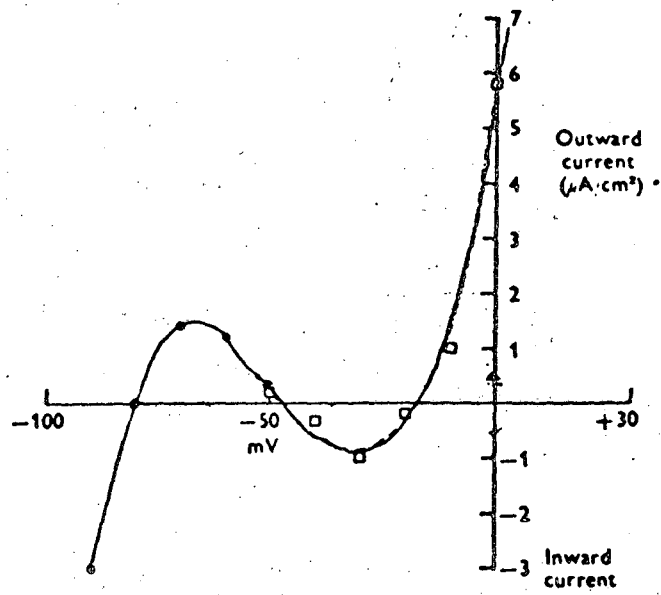
Instantaneous Current-Voltage Relation

Figure A4

from page 225 of (16)
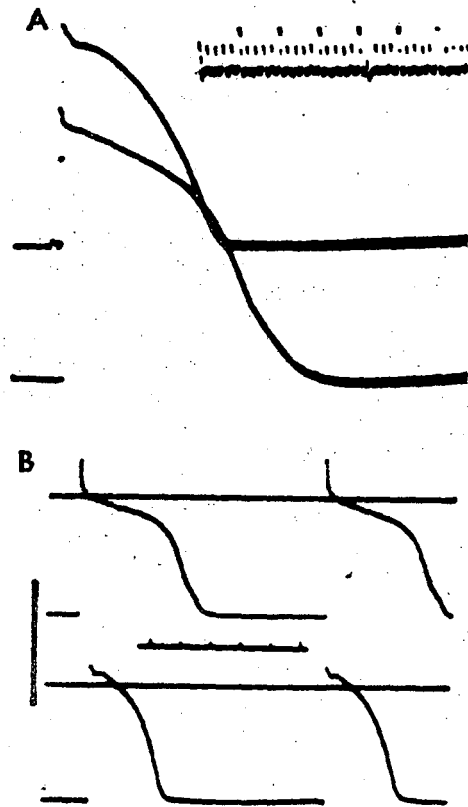
Recorded Purkinje Fiber Action Potentials

FIG. 7-1. (A) Transmembrane action potentials recorded from papillary muscle (top trace) and attached Purkinje fibers (bottom trace) of the dog right ventricle. Time calibration shows intervals of 10 and 50 msec. (B) Transmembrane action potentials recorded from papillary muscle (bottom) and isolated false tendon (top) of the dog left ventricle. Upper trace in both records is the line of zero potential. Time calibration shows intervals of 100 and 500 msec. Vertical bar at left of figure is a voltage calibration of 100 mv for B.

Figure A5

from page 177 of (3)

Records of Oscillatory Activity

Seconds
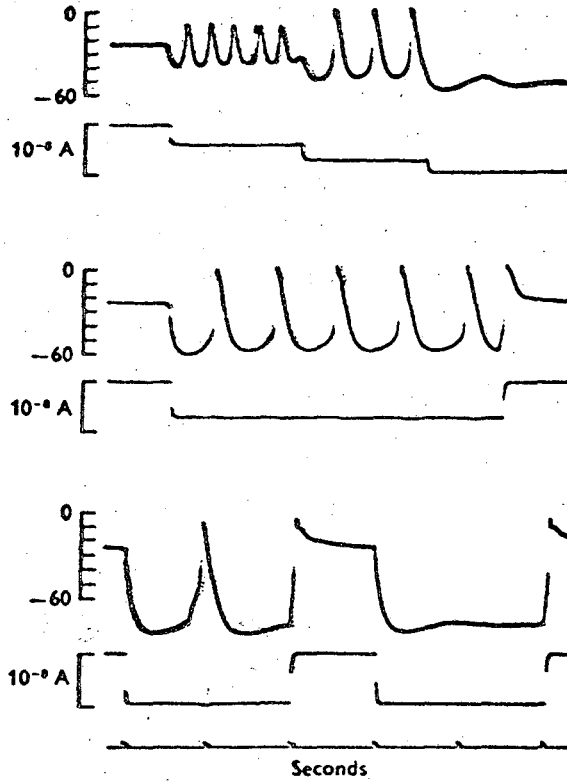
Figure A6

from page 262 of (12)

An Example of Stiffness Instability in
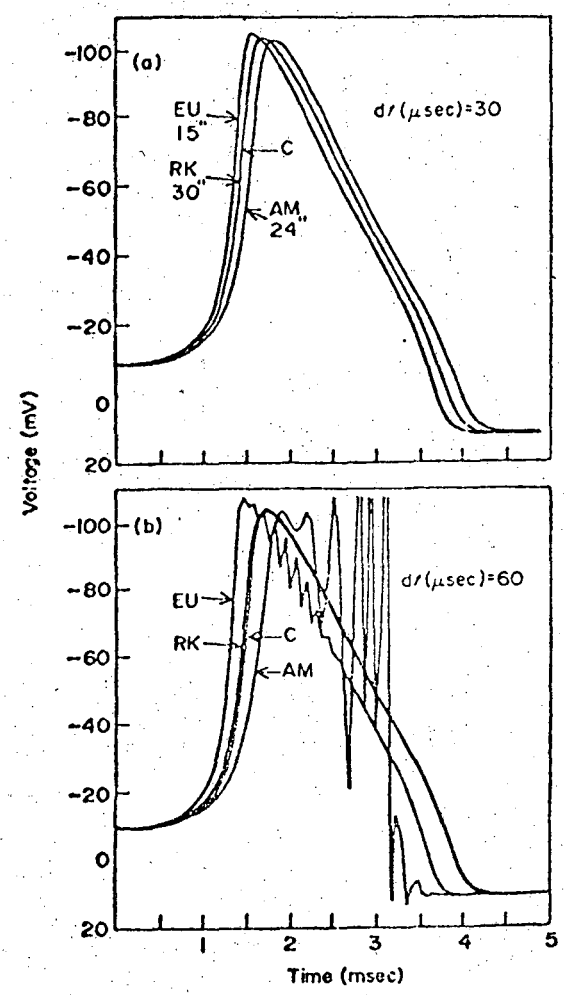The Integration of the Hodgkin-
Huxley Equations

Fig. 2. (a) Comparison of H-H action potentials generated by the Euler (EU), Runge-Kutta (RK), and Adams (AM) integration methods for a 30 µsec time step with a convergent solution (C). The corresponding computation and plotting time are shown in seconds. (b) As for (a), except that integration step size doubled to 60 µsec.

Figure A7
from page 260 of (15)